10/3-24-97 JSD (1)

SAND--97-8227

M9705218?

SANDIA REPORT

SAND97-8227 • UC–411
Unlimited Release
Printed February 1997

The Chemistry of Halogens on Diamond: Effects on Growth and Electron Emission

C. A. Fox, W. L. Hsu, M. E. Coltrin, L. S. Pan, L. A. Brown, M. A. Kelly, S. B. Hagstrom, S. T. Bosson, R. Cao, G. Vergara, and M. C. McMaster

Prepared by
Sandia National Laboratories
Albuquerque, New Mexico 87185 and Livermore, California 94551
for the United States Department of Energy
under Contract DE-AC04-94AL85000

Approved for public release; distribution is unlimited.

Issued by Sandia National Laboratories, operated for the United States Department of Energy by Sandia Corporation.

Available to DOE and DOE contractors from:

Office of Scientific and Technical Information
P.O. Box 62
Oak Ridge TN 37831

Prices available from (615) 576-8401, FTS 626-8401.

Available to the public from:

National Technical Information Service
U.S. Department of Commerce
5285 Port Royal Rd.
Springfield, VA 22161

SAND97-8227 UC-411
Unlimited Release
Printed February 1997

THE CHEMISTRY OF HALOGENS ON DIAMOND: EFFECTS ON GROWTH AND ELECTRON EMISSION

C.A. Fox[c], W.L. Hsu[a], M.E. Coltrin[b], L.S. Pan[a], L.A. Brown[a], M.A. Kelly[c], S.B. Hagstrom[c], S.T. Bosson[a], R. Cao[d], and G. Vergara[e], M. C. McMaster[a]

[a]Sandia National Laboratories, Livermore, CA
[b]Sandia National Laboratories, Albuquerque, NM
[c]Department of Materials Science and Engineering, Stanford University
[d]Stanford Synchnotron Radiation Laboratory
[e]Electrical Engineering Department, Stanford University

ABSTRACT

The feasibility of diamond growth using halogenated precursors was studied in several diamond growth reactors. In a conventional microwave plasma reactor, diamond growth using the following gas mixtures was studied: CF_4/H_2, CH_4/H_2, CH_3F/H_2, and CH_3Cl/H_2. Both the diamond growth measurements (film growth rate, film quality, etc.) and *in-situ* near-surface gas composition measurements demonstrated ineffective transport of halogen radicals to the diamond surface during the growth process. In order to transport radical halogen species to the diamond surface during growth, a flow-tube reactor was constructed which minimized gas phase reactions. In addition, the flow-tube reactor enabled pulsed gas transport to the diamond surface by fast-acting valves. Molecular beam mass spectroscopy was used to find conditions which resulted in atomic hydrogen and/or atomic fluorine transport to the growing diamond surface. Although such conditions were found, they required very low pressures (.5 Torr and below); these low pressures produce radical fluxes which are too low to sustain a reasonable diamond growth rate. Due to the limitations of both the conventional plasma reactor and the flow-tube reactor, the sequential reactor at Stanford University was modified to add a halogen-growth step to the conventional atomic hydrogen/atomic carbon diamond growth cycle. Since the atomic fluorine, atomic hydrogen, and atomic carbon environments are independent in the sequential reactor, the effect of fluorine on diamond growth could be studied independently of gas phase reactions. Although the diamond growth rate was increased by the use of fluorine (compared to growth without fluorine under similar conditions), the film quality was seen to deteriorate as well as the substrate surface. Moreover, materials incompatibilities with fluorine significantly limited the use of fluorine in this reactor.

A diamond growth model incorporating both gas phase and surface reactions was developed for the halocarbon system concurrent with the film growth efforts. In this report, we review the results of the growth experiments, the modeling, and additional experiments done to understand fluorine interaction with diamond surfaces. In addition, fluorine modification of diamond surfaces after growth is used to prepare cesiated-diamond cathodes which have field emission characteristics that are both air stable and thermally stable (200°C).

Introduction

In the past twenty years, researchers have developed a host of techniques to deposit polycrystalline diamond films. Researcher's interest in diamond films originates from the unique physical and chemical properties of diamond. Diamond has the highest thermal conductivity. Diamond's wide optical transmittance coupled with its high strength make it an ideal material for high vacuum optical windows.[1] Diamond films have been used to extend the lifetime of cutting tools; here, diamond's hardness and chemical inertness are critical. Diamond is the ideal material for high-power high-frequency devices because of its relatively large electron and hole mobilities and a relatively low dielectric constant.[2] Diamond devices might also be expected to withstand higher temperatures than analogue silicon devices. Diamond films are also candidate field emission materials (FEM) due to diamond's high thermal conductivity and low surface work function.[3] The large thermal conductivity of diamond enables the cathode to draw large currents and dissipate the heat generated by these currents. Although the high thermal conductivity and low work function are compelling reasons for using diamond as a field emission material, probably the most often invoked reason for pursuing diamond as a FEM is the negative electron affinity (NEA) property of specially-prepared diamond surfaces.[4,5] Despite many of its material properties, there are few practical diamond devices (with the exception of particle detectors) available which exploit the electronic properties of diamond because of several limitations in diamond growth. Although significant advances have been made in some areas of diamond film growth, several fundamental drawbacks inhibit widespread application of chemically-vapor deposited films.

The high substrate temperature required to deposit diamond (600-1000°C) is a major impediment not only for diamond-based field emitters, but for most diamond applications in general. These high temperatures not only prevent the deposition of thin diamond films onto glass substrates which may be used in FED displays, but in addition, increase the complexity of diamond growth reactors. The high temperatures required for diamond growth are similarly not compatible with many materials involved in integrated circuits. Nucleation limitations also drastically limit diamond growth on substrates used in flat panel displays. Although recent studies have demonstrated the possibility of overcoming the diamond nucleation barrier on non-native substrates using an ion-assisted process,[6-9] the applicability of this process to insulating substrates is unclear. Almost irrespective of the growth technique, the high cost of depositing diamond further complicates manufacturing of diamond-based field emitters. Both the costs and surface temperature limitations are related to the surface processes involved in conventional, hydrocarbon/hydrogen based diamond growth. The reliance on atomic hydrogen, for almost all diamond deposition technologies, controls both the surface temperatures required for growth and the costs.

Recently, there has been interest in developing diamond growth processes with reduced reliance on atomic hydrogen by incorporating halogens into the chemical vapor deposition process. These precursors may produce gas-phase diamond growth species other than the methyl radical which could facilitate diamond growth. Such a likelihood was suggested in the experiment by Hukka *et al* to deposit diamond by alternating exposure of a diamond crystal to a halocarbon and atomic hydrogen.[10,11] Halocarbon precursors may enable the use of halogen-hydrogen abstraction reactions to sustain diamond growth. Work of other researchers suggests that alternative halocarbon chemistries might enable diamond growth at reduced temperatures without a simultaneous deterioration in deposit quality or growth rate.[12,13] Recent *ab initio* calculations suggest that high quality diamond films can

be grown in an atomic layer epitaxy process involving exposure of gaseous hydrocarbons and fluorocarbons to a hydrogenated or fluorinated diamond (110) surface.[14]

Lower growth temperatures and reduced nucleation barriers have been reported by researchers using halogen-assisted diamond growth processing. Rudder *et al.*, claimed diamond films deposited from 8%CF_4/H_2 gas mixtures using radio-frequency discharges.[15] Rudder also reported success using mixtures of CH_4/F_2 in a thermal system (oven) without nucleation pretreatment. Kadono *et al.*, used CF_4/H_2 precursor gas mixtures in microwave-assisted plasma diamond deposition (MPCVD) and observed difluoromethylene ($CF_2^{\bullet}$) and trifluoromethyl ($CF_3^{\bullet}$) intermediates in the gas phase by optical emission spectroscopy; however, they did not determine the importance of these species to the diamond growth process.[16]

Unfortunately, much of the early studies into halogenated film growth have not been repeated. Moreover, recent reports suggest that atomic fluorine is deleterious to diamond growth[17] while significant coverages of chlorine on diamond surfaces are not feasible.[14,18] Maeda *et al.*, reported the effect of increasing the fluorine input on the activation energy for diamond growth in MPCVD using CF_4/H_2, CHF_3/H_2, and CH_4/H_2 gas mixtures.[17] The activation energies for diamond growth in the temperature range 640-850°C were measured to be 28.4 kcal/mole, 20.5 kcal/mole, and 10.3 kcal/mole, respectively. Based on these activation energies, the authors concluded that the surface reaction mechanism of fluorocarbon systems is different from that of hydrocarbons, and that fluorine atoms would actually inhibit diamond growth.

It is clear from this brief literature review that the effect of halogen species incorporation on the gas-phase and surface chemistry of CVD diamond growth is not well understood. To understand the incorporation of halogens into the diamond growth process, a three-step approach was adopted. First, plasma, thermodynamic and kinetic calculations were done to demonstrate the feasibility of a hybrid atomic fluorine/atomic hydrogen diamond growth process. If atomic hydrogen abstraction to create open-sites and incorporate carbon into the diamond lattice is the process that prevents diamond growth at reduced surface temperatures, then a hybrid atomic fluorine and atomic hydrogen process which exploits halogen abstraction may be more suited for lower temperature diamond growth. Secondly, diamond growth experiments using fluorinated precursors was done in a conventional, microwave plasma diamond deposition system. These experiments were done to test the introduction of halogens into diamond growth systems. Due to the limitations of halogen transport to the diamond surface in a conventional, diffusion-controlled reactor, alternative reactors were studied to transport halogen radicals to the diamond surface during growth. Although the use of halogens during diamond growth process was very limited in all three reactors for various reasons, atomic fluorine modification of *as-grown* diamond surfaces after growth was possible using a plasma reactor. In the third section of this report, fluorine modification of diamond surfaces was used as a processing step to enhance the field emission from diamond surfaces. This processing step facilitated low-temperature bonding of cesium to previously hydrogenated carbon surfaces.

Thermodynamic and Kinetic Calculations of Diamond Growth

Modeling Microwave Plasma Experiments

In an attempt to determine the relative importance of neutral-neutral reactions in a MPCVD reactor, we have used a numerical model based solely on thermal chemistry to simulate the reaction environment used in this study. The formalism for this model was developed by Coltrin and coworkers.[42,43] A detailed description of the model formulation has been previously reported,[42] so we present a brief summary here of its more salient features. The program models a one-dimensional stagnation flow through a "reaction zone" representative of the region from the point where the gas is activated (in these calculations, the gas is activated at the plasma "center") to the growth surface; three dimensional effects are not included. Thermodynamic and chemical information is provided by the CHEMKIN[44] and Surface CHEMKIN packages.[43] The reaction mechanism[45] incorporates the kinetics of 34 homogeneous reactions; no plasma effects (such as ion-neutral or electron-neutral reactions) are included. The heterogeneous reaction kinetics include 24 heterogeneous reactions involving C_1 and C_2 species with the growth surface; reactions on the cold reactor walls are not included since the model assumes all surface reactions occur on the stagnation plane. Using this formalism, we have been able to quantitatively predict the near-surface gas composition in a hot-filament chemical vapor deposition (HFCVD) reactor under reaction conditions where diamond growth occurs (carbon mole fraction (X_C) $\leq$ 0.02).[46,47] The ability of this model to predict the hydrocarbon product distribution when filament poisoning effects are negligible suggests that the neutral-neutral homogeneous hydrocarbon chemistry is well understood.

The model has several input parameters, including the reactor pressure, the surface temperature, the axial velocity at the inlet of the reaction zone, the inlet composition, the inlet gas temperature and the reaction distance. The reactor pressure and surface temperature were set equal to their experimental values. For these simulations, the axial velocity at the inlet of the reaction zone is set to 1 cm/s as estimated from experimental conditions. Since diffusion dominates mass transport under these conditions, the exact the axial velocity has no impact on the results. The composition of the gas entering the reaction zone was set equal to the composition of the gas stream fed to the reactor. Since direct dissociation of H_2 to H atoms by electrons may be equally as important as thermally-induced dissociation in the microwave plasma system, the H-atom mole fraction at the inlet to the reaction zone is also an input parameter. Since we do not know the H-atom mole fraction in this region, we choose a value such that the simulations yield a H-atom mole fraction at the gas-surface interface that is close to the H-atom mole fraction measured experimentally. For these simulations, the H-atom mole fraction at the inlet was set to 0.03. The inlet gas temperature (1700 K) and reaction distance (13 mm) were set equal to the values used in the previous modeling of the HFCVD experiments.[46] This value of the gas temperature is consistent with the gas temperatures measured in weakly ionized plasmas (1100 to 2000 K).[48,49]

Although the model is able to reproduce some features observed experimentally, it is generally unable to simulate the near-surface gas composition measured in the plasma environment. As the acetylene concentration in the feed increases, the model predicts increases in the mole fractions of all the hydrocarbon species (Fig. 1). Although the C_2H_2,

CH_3 and H-atom mole fractions are in quantitative agreement with experiment, the mole fractions of other hydrocarbons are not. For example, the predicted CH_4 mole fraction is 2 to 3 times too low and the C_2H_4 mole fraction is an order of magnitude too large. The large amount of C_2H_6 predicted at larger values of X_C is particularly surprising since no ethane was detected in the experiment at any C/H ratio. When the calculations are repeated with methane in the feed, differences between the model and experiment are larger. Changing the values of the input parameters does not improve the agreement between the model predictions and the experimental results; a sensitivity analysis indicated that the values selected for these parameters were optimal. Not only does the model incorrectly calculate the near-surface gas composition generated using either carbon source, it also cannot account for the insensitivity of the gas composition to the identity of the hydrocarbon source. This insensitivity to the starting reagent observed experimentally suggests the microwave plasma initially converts either source gas into a mixture of species that is determined only by the C/H ratio in the feed. Thus, with the same starting material in each system, subsequent reaction processes create a near-surface gas composition that is a function only of X_C. To include this possibility into the model, we performed a calculation assuming the inlet carbon source is immediately decomposed to atomic carbon and hydrogen. Then we allowed the numerical simulation to calculate the gas composition as before. This effort produces only minimal improvement in the calculated result; the ethylene and ethane mole fractions are much larger than measured experimentally.

Although the plasma system is inherently three dimensional, at the region where the plasma makes contact with the wafer the geometry is relatively more planar than for the hot-filament case. In that situation, the model can simulate the chemically reacting environment of a methane/hydrogen mixture quite well, therefore, we do not believe the discrepancies between the model and experimental results originate from three dimensional transport effects.[46]

The simulations we have performed in this study demonstrate that neutral-neutral interactions are insufficient to characterize the microwave plasma-assisted reaction environment over a broad range of conditions. We believe future attempts to model the plasma-assisted reaction environment must include ion-neutral and electron-neutral chemistry.

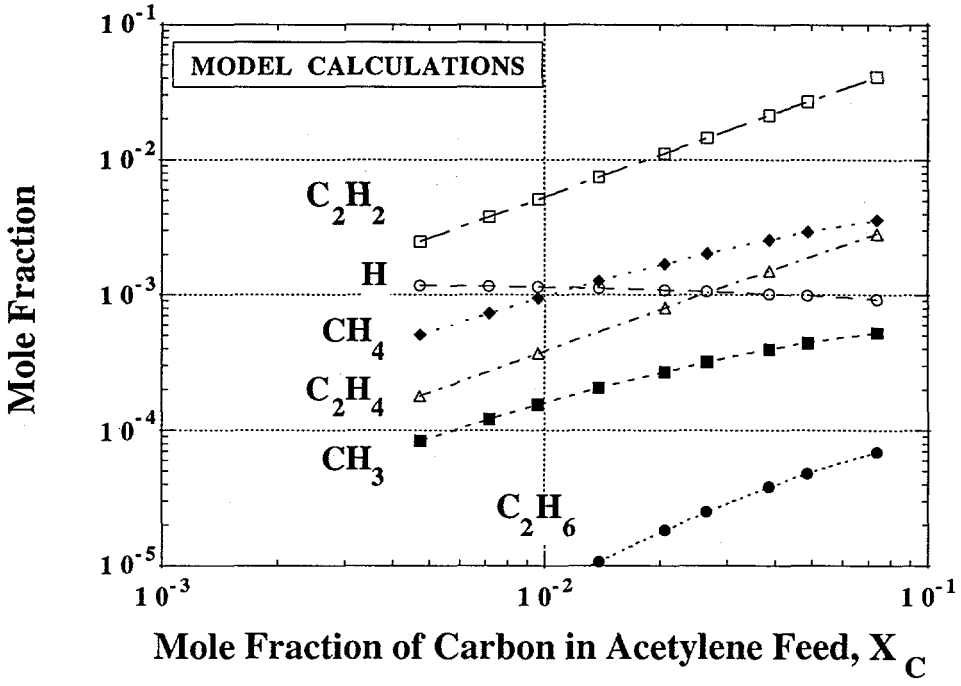

Figure 1: Numerical model calculations of the species mole fractions at the near-surface region versus the carbon mole fraction in a acetylene feed. Inputs for the surface temperature, gas temperature and pressure were at 825°C, 1425°C and 20 Torr, respectively.

Modeling CF_4 / H_2 Reacting-Flow System

We have also worked on a reaction mechanism for the deposition of diamond from halogen sources, using CF_4 / H_2 as a prototype system. An extensive literature survey was conducted to find chemical reaction kinetics and thermochemical data. From this, a detailed gas-phase reaction mechanism consisting of 24 reversible chemical reactions for the decomposition of CF_4 in a mixture of H and H_2 was constructed. This gas-phase reaction mechanism is listed in Table 1. The mechanism was tested using the SENKIN gas-phase kinetics code.[50]

Transport properties (in the form of Lennard-Jones intermolecular potentials) for the 14 species in the gas-phase reaction mechanism were also assembled. These properties are needed to do the full chemically reacting flow simulations of a diamond flow tube reactor. Potentials were available from the literature for the species C, CF, CF_2, CF_3, CF_4, CH_2CF_2, CHF_3, H, F, HF, F_2, and H_2. Properties for C_2F_4 and C_2F_6 were estimated by analogy with hydrocarbon species. The transport parameters are listed in Table 2.

A simple analysis of the thermochemistry and kinetics of diamond surface species in the fluorocarbon system was performed. By analogy with gas-phase bond strengths and our early work on diamond modeling, the surface C-F bond strength was estimated to be 120 kcal/mole. By contrast, the surface C-H bond strength is about 95 kcal/mole. From this information, a simple surface reaction mechanism consisting of three surface species,

CF(s), CH(s), and C(s,r) (a surface radical species) and 6 reversible reactions was constructed, i.e., reactions of H and F with each of the three surface species.

All of the above work was combined into a realistic simulation of the coupled gas-phase chemistry, surface chemistry and fluid flow in a diamond hot-filament reactor using a CF_4 source under typical reactor conditions. The inlet composition (actually the assumed composition at the filament) was 1% CF_4, 2.5% H, and 96.5% H_2. Plotted in Figure 2 are the gas-phase mole fractions predicted by the model as a function of height above the substrate. One sees rapid recombination (destruction) of the gas-phase H atoms, but little decomposition of the CF_4. The calculated rise in CF_4 at the surface is due to the physical effect of thermal diffusion. The model predicts that the surface composition is roughly 85% CH(s), 15% C(s,r), and only 1.0E-6% CF(s).

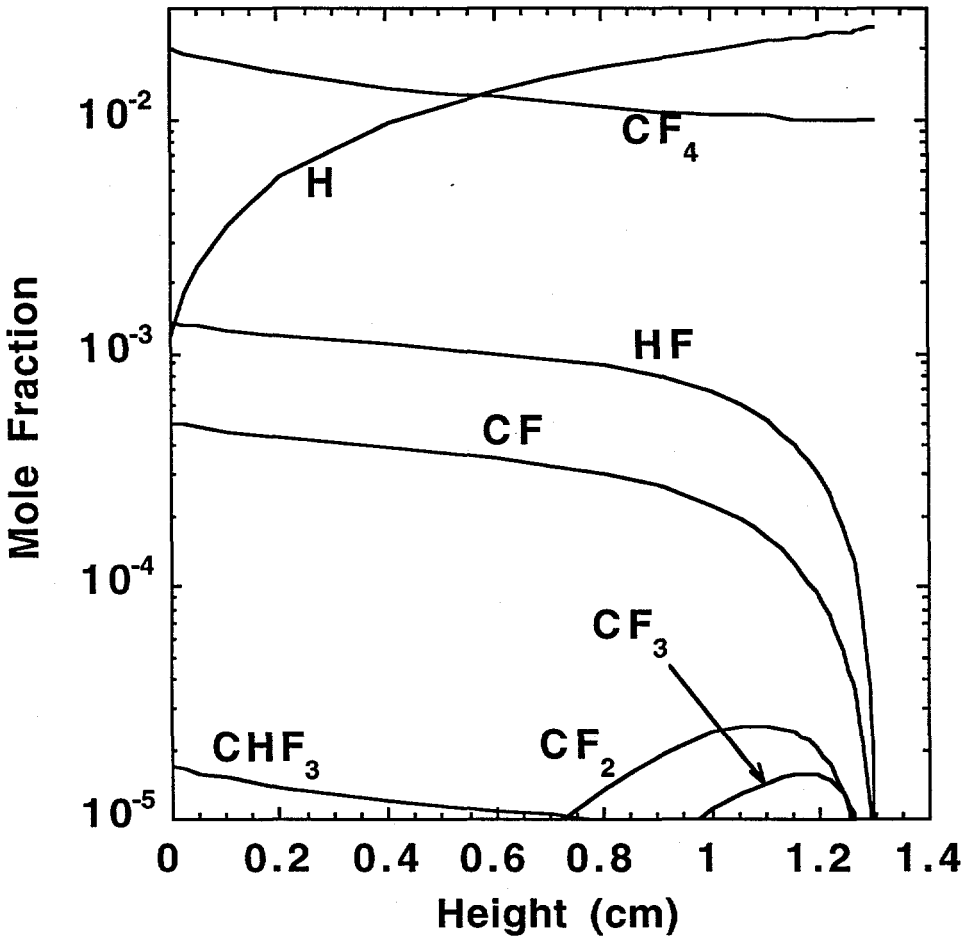

Figure 2: Numerical model calculations of the species mole fractions versus height above the reacting surface. Inputs for the surface temperature, gas temperature and pressure were at 825°C, 2325°C and 20 Torr, respectively.

Table 1. Gas-phase reaction mechanism for the C/H/F system.
Reaction rate = A (T^{β}) exp(-Act. Energy/RT).

Reaction	A[(a)]	β	Act. Energy[(b)]	Ref.
$F+CF \leftrightarrow F_2+C$	6.38E+13	0	71550	54
$CF+M \leftrightarrow C+F+M$	3.00E+15	0	111000	55
$CF_2+H_2 \leftrightarrow CH_2F_2$	6.02E+07	0	0	56
$CF_2+H \leftrightarrow CF+HF$	2.35E+13	0	0	57
$CF+F_2 \leftrightarrow CF_2+F$	1.00E+12	0	0	55
$CF_2+CF_2 \leftrightarrow C_2F_4$	4.34E+10	0	0	58
$CF_2+M \leftrightarrow CF+F+M$	4.20E+26	-2.85	106000	59
$CF_2+F_2 \leftrightarrow CF_3+F$	1.98E+11	0.5	2120	60
$CF_3+H \leftrightarrow CF_2+HF$	5.48E+13	0	0	61
$CF_3+H+M \leftrightarrow CHF_3+M$	2.00E+20	-1	0	62
$CHF_3+H \leftrightarrow H_2+CF_3$	3.20E+12	0	11200	63
$CHF_3+F \leftrightarrow CF_3+HF$	1.00E+12	0	3000	55,64
$CF_3+F_2 \leftrightarrow CF_4+F$	9.03E+11	0	0	65
$CF_3+M \leftrightarrow CF_2+F+M$	1.57E+49	-9.04	92254	60
$CF_3+CF_3 \leftrightarrow C_2F_6$	2.11E+12	0	0	66
$CF_4+M \leftrightarrow CF_3+F+M$	6.15E+34	-4.64	122421	60
$CF_4+H \leftrightarrow CF_3+HF$	7.10E+14	0	43700	67
$H+HF \leftrightarrow F+H_2$	1.65E+12	0.6	32510	68
$F+HF \leftrightarrow F_2+H$	1.33E+13	0	100710	69
$C+HF \leftrightarrow CF+H$	2.99E+13	0	39280	54
$F_2+M \leftrightarrow F+F+M$	1.52E+12	0	23920	70
$H+F+M \leftrightarrow HF+M$	4.91E+15	0	-3050	71
$H+H+M \leftrightarrow H_2+M$	1.00E+18	-1	0	72
$H+H+H_2 \leftrightarrow H_2+H_2$	9.20E+16	-0.6	0	72

(a) Units depend upon reaction order, but are given in terms of moles, cm^3, and sec.

(b) cal/mole

Table 2. Lennard-Jones transport parameters; σ is the collision diameter, and ε/k is the well-depth where k is the Boltzmann constant.

Molecule	σ (Å)	ε/k (K)	Ref.
CF	3.635	94.2	73
CF_2	3.977	108	73
CF_3	4.32	121	73
CF_4	4.662	134	73
CH_2F_2	4.08	318	73
CH_4	3.758	148.6	73
CH	3.37	68.6	73
C_2H_4	4.163	224.7	73
C_2H_2	4.033	231.8	73
C_2H_6	4.443	2.157	73
CHF_3	4.33	240	73
C_2F_6	5.512	194.5	55
C_2F_4	5.164	202.6	55

Table 3. Surface reaction mechanism for the C/H/F system.

Reaction	Probability[(a)]
CH(s)+H↔C(s,r)+H2	0.1
CH(s)+F↔C(s,r)+HF	1.0
CF(s)+H↔C(s,r)+HF	1.0
CF(s)+F↔C(s,r)+F2	1.0E-10
C(s,r)+H↔CH(s)	0.3
C(s,r)+F↔CF(s)	0.3

(a) Unitless

Molecular Mechanics Calculations

We used a molecular mechanics program[51-53] (MM3) to calculate thermochemical information (heats of formation, entropy, and heat capacity as a function of temperature) for surface species relevant to halogen diamond CVD. The MM3 program had not been parameterized for calculations of halogenated species. We carried out this task by calibrating the calculated heats of formation to the reference species: Methyl-X, Ethyl-X, Isopropyl-X, and Tertiarybutly-X (X=F, Cl, Br, I).

Using the halogen bond-energy parameters, the energetics for the hydrogenated surfaces of diamond were calculated for the dimerized 2x1:(100), (110), and (111) crystal faces. (The starting surface is denoted as the species "slab" in the following tables.) For these calculations, one of the hydrogens on the surface was (1) removed to create the radical structure (which we denote "slabR"), and then (2) replaced by one of the following:

F, Cl, Br, I, OH, or CH_3. In this manner, we obtained the heats of formation for the surface radical and the various substituted lattices (see Table 4). This information was then used to calculate the heats of reaction for various types of gas/surface reactions for each of the three crystal faces. These reaction energetics are summarized as Tables 5-8, below.

Table 4. Heats of formation for surface structures[(a)].

Species	100 Face	110 Face	111 Face
slab	0.00	0.00	0.00
slabR	48.68	41.46	45.58
slabF	-50.59	-48.03	-52.57
slabCL	-7.81	5.43	-6.24
slabBR	7.12	21.26	7.10
slabI	17.47	34.25	21.54
slabOH	-37.47	-33.49	-37.50
slabCH_3	0.12	16.00	1.91

(a) kcal/mole

Table 5. Heats of reaction[(a)] for CH(s)+X ↔ C(s,r)+HX

X	100 Face	110 Face	111 Face
H	-3.39	-10.61	-6.49
F	-35.29	-42.51	-38.39
CL	-2.36	-9.58	-5.46
BR	15.10	7.88	12.00
I	29.44	22.22	26.34
OH	-18.41	-25.63	-21.51
CH_3	-4.01	-11.23	-7.11

(a) kcal/mole

Table 6. Heats of reaction[(a)] for CX(s)+H ↔ C(s,r)+HX

X	100 Face	110 Face	111 Face
H	-3.39	-10.61	-6.49
F	-17.92	-27.70	-19.04
CL	-17.64	-38.10	-22.31
BR	-17.35	-38.71	-20.43
I	-14.56	-38.56	-21.73
OH	-23.70	-34.90	-26.77
CH_3	-21.40	-44.50	-26.29

(a) kcal/mole

Table 7. Heats of reaction[(a)] for C(s,r)+X ↔ CX(s)

X	100 Face	110 Face	111 Face
H	-100.75	-93.53	-97.65
F	-118.12	-108.34	-117.00

CL	-85.47	-65.01	-80.80
BR	-68.30	-46.94	-65.22
I	-56.75	-32.75	-49.58
OH	-95.46	-84.26	-92.39
CH_3	-83.36	-60.26	-78.47

(a) kcal/mole

Table 8. Heats of reaction[(a)] for $CX(s)+X \leftrightarrow C(s,r)+X_2$

X	100 Face	110 Face	111 Face
H	-3.39	-10.61	-6.49
F	80.42	70.64	79.30
CL	27.51	7.05	22.84
BR	14.82	-6.54	11.74
I	5.67	-18.33	-1.50

(a) kcal/mole

Thermodynamic and Kinetic Calculations of Abstraction Processes in Diamond Growth

In the previous section, molecular mechanics was used to calculate thermodynamic properties of fluorine and hydrogen on diamond surfaces. In this section, these quantities are used to assess of the thermodynamics of diamond growth in the carbon, hydrogen, and fluorine system.

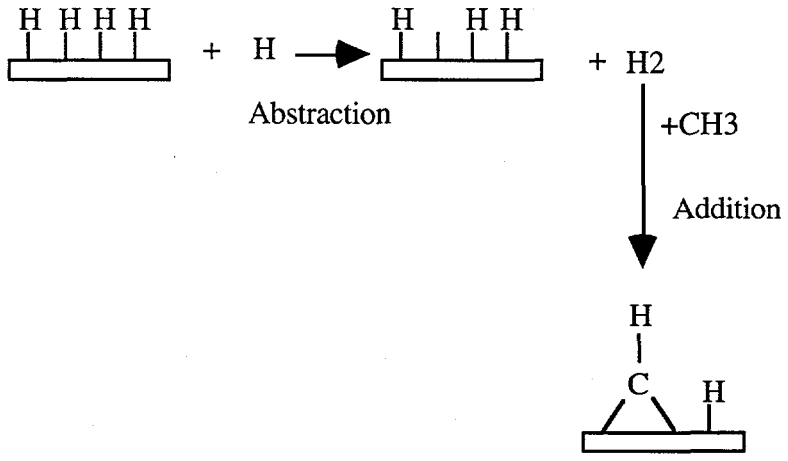

Figure 3 - Schematic diagram of the chemical processes occurring during diamond growth from atomic hydrogen and methyl radical gas mixtures.

The abstraction process shown in Figure 3 has been considered by various researchers, including Harris[19] and Coltrin. Using molecular mechanics, Coltrin calculated thermochemical information related to halogen diamond CVD (see previous section). For

the abstraction reaction illustrated in Figure 3, the enthalpies were -3.39, -10.61, and -6.55 kcal/mole, for the (2x1):C(100), 1x1:C(110), and 1x1:C(111) surfaces, respectively. The negative abstraction enthalpy for these crystal surfaces indicates that this reaction is thermodynamically exothermic. However, it is important to note that only the bond enthalpy was calculated and hence entropic considerations were ignored; this thereby prevents direct calculation of the Gibbs Free Energy which is typically used to determine if a process is thermodynamically favorable.

The Gibbs free energy for the abstraction of a surface hydrogen can be calculated using the thermochemical values for the hydrogenated surface calculated by Harris using molecular mechanics. These values were calculated for the hydrogenated C(111) surface based on the group additivity technique and take into consideration steric hindrances between neighboring hydrogen atoms on the hydrogen-terminated C(111) surface. The hydrogen abstraction of hydrogen to create a radical site (e.g. open-site) is thermodynamically favorable across the entire temperature range shown in Figure 4. Although this was only done for the C(111) surface, similar dependencies can be expected for the other low index diamond surfaces since the entropic contribution is smaller than the enthalpic contribution when the gas phase species moles are unchanged (by the abstraction reaction).

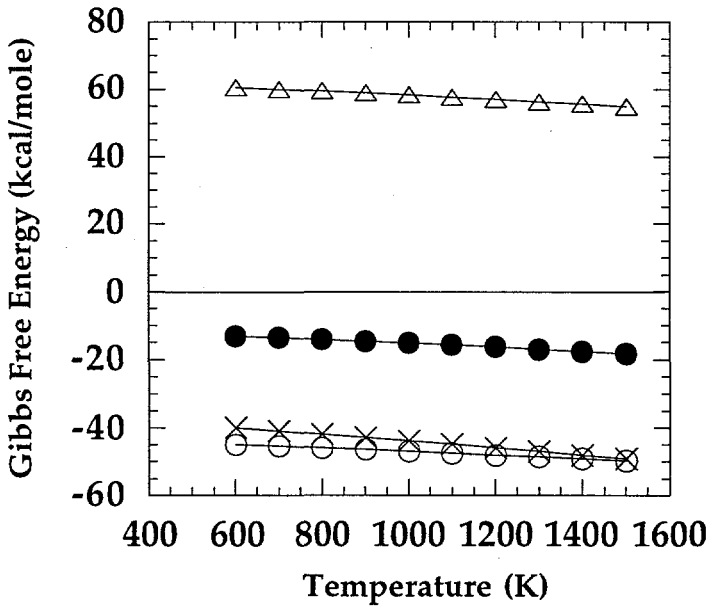

Figure 4 - Gibbs Free energy of reaction for atomic hydrogen abstractions and atomic fluorine abstractions from the C(111) surface based on thermochemical values calculated by Harris. The hydrogen abstraction of hydrogen (filled circles), the hydrogen abstraction of fluorine (x's), the fluorine abstraction of fluorine (triangles), and the fluorine abstraction of hydrogen (open circles) are shown as a function of the surface temperature.

In Figure 5, an analogous diamond growth process is illustrated using atomic fluorine rather than atomic hydrogen to create radical sites and stabilize the diamond surface configuration. For the fluorine-based process show in Figure 5, growth sites are created by atomic fluorine abstraction of atomic fluorine from the diamond surface yielding a radical site and gas phase molecular fluorine. In the process illustrated in Figure 5, the other reactions required to incorporate the CF_x radicals into the diamond lattice are ignored;[21] in addition, the problem of generating gas phase CF_x radicals and/or atomic

fluorine is not discussed. Since the abstraction reaction yields molecular fluorine, a relatively weakly bonded molecule, it is highly endothermic. For the diamond (100), diamond(110), and diamond (111) surfaces, the formation reaction enthalpies are 80.4, 70.7, and 79.2 kcal/mole. Since the entropic contribution is still small compared to the bond enthalpies, the Gibbs Free energy of the abstraction process is expected to be positive; consequently, the abstraction reaction is not thermodynamically favorable. The Gibbs free energy of the fluorine abstraction of fluorine is shown in Figure 4 for the C(111) surface; here, the abstraction process is highly endothermic (>55 kcal/mole) across the entire temperature range indicating that this process for radical-site creation is highly unlikely on the fluorinated C(111) surface.

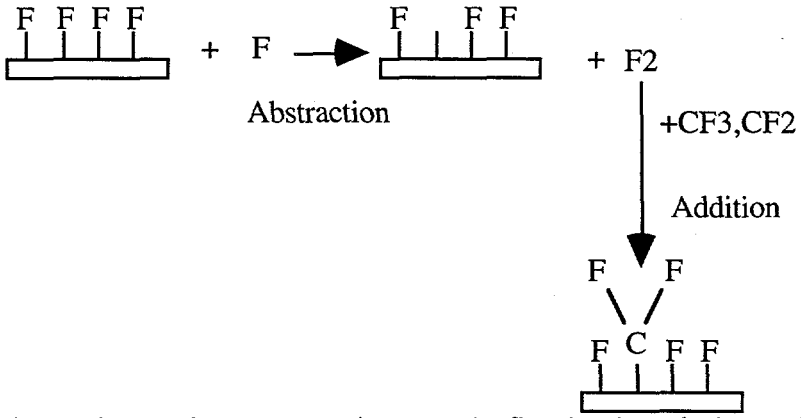

Figure 5. Diamond growth process using atomic fluorine-based abstraction reactions to create open sites for carbon addition. Although carbon addition is shown using CF_2 and CF_3 radicals, carbon atom addition is also viable.

Another potentially useful halogen for diamond growth is chlorine. Similar to the fluorine-based process shown in Figure 5, the abstraction enthalpies for chlorine abstraction of chlorine from a diamond surface are also positive (e.g. endothermic), although not as positive as the case of fluorine. The enthalpies are 27.5, 7.05, and 22.8 kcal/mole, for the diamond (100), diamond (110), and diamond (111) surfaces, respectively. Based on these results, a solely halogen process using a either fluorine or chlorine and carbon would not be expected to grow diamond.

However, the energetics of a hybrid diamond growth process using both atomic hydrogen and a halogen are significantly more favorable. In Figure 6, such a growth process is illustrated. Here, radical-sites for carbon addition are created via the following abstraction reactions: 1) atomic fluorine abstraction of atomic hydrogen; 2) atomic hydrogen abstraction of atomic hydrogen; 3) and atomic hydrogen abstraction of atomic fluorine. Due to large bond strength of molecular HF, reactions (1) and (2) are strongly favored. Coltrin calculated heats of reaction of -17.92, -27.70, and -19.4 kcal/mole for reaction (2) for the C(100), 1x1:C(110), and the 1x1:C(111) surfaces, respectively. The calculated heats of formation for reaction (1) were even more favorable: -35.29, -42.51, and -38.39, kcal/mole, for the C(100), 1x1:C(110), and the 1x1:C(111) surfaces, respectively. Similar to the fluorinated case, the hybrid halogen process using chlorine is also favorable, albeit the heats of reaction are less negative. However, recent *ab initio* calculations indicate that the steric interactions between chlorine atoms limits the coverage of chlorine on diamond surfaces;[14] the limited coverage of chlorine on the diamond(100)

and (111) surfaces was recently confirmed.[18] The Gibbs free energy for the hydrogen and fluorine respective abstractions are shown in Figure 4. These abstractions are thermodynamically the most favorable and argue that a diamond growth process using both atomic fluorine and atomic hydrogen to create radical sites for carbon addition may be promising route toward diamond deposition at low substrate temperatures.

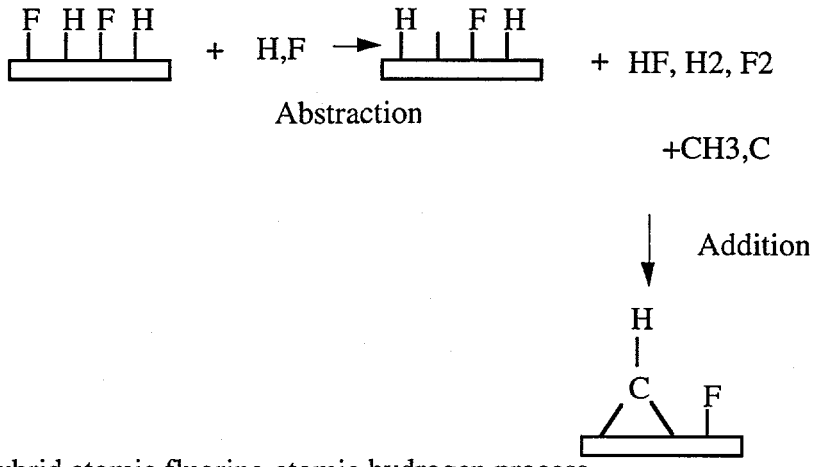

Figure 6 - Hybrid atomic fluorine-atomic hydrogen process.

When fluorine and hydrogen are used simultaneously in the thermodynamically favorable hybrid growth process, the open-site concentration is determine both by atomic hydrogen and atomic fluorine abstractions. In this case, the following reaction set must be evaluated:

$$C^H + H_{gas} \leftrightarrow C^* + H_{2gas} \qquad k_1^f \qquad (9)$$

$$2C^* + 2H_{gas} \leftrightarrow 2C^H \qquad k_2^f \qquad (10)$$

$$C^H + F_{gas} \leftrightarrow C^* + HF_{gas} \qquad k_3^f \qquad (11)$$

$$C^F + H_{gas} \leftrightarrow C^{\bullet} + HF_{gas} \qquad k_4^f \qquad (12)$$

$$2C^* + 2F_{gas} \leftrightarrow 2C^F \qquad k_5^f \qquad (13)$$

$$C^F + F_{gas} \leftrightarrow C^* + F_{2_{gas}} \qquad k_6^f \qquad (14)$$

$$C^H + C^F \leftrightarrow 2C^* + HF_{gas} \qquad k_7^f \qquad (15)$$

$$C^F + C^F \leftrightarrow 2C^* + F_{2_{gas}} \qquad k_8^f \qquad (16)$$

$$C^H + C^H \leftrightarrow 2C^* + H_{2_{gas}} \qquad k_9^f \qquad (17)$$

In this reaction set, three surface species are pertinent: carbon bonded to hydrogen (C^H), carbon bonded to fluorine (C^F), and open-sites (C^*). Reaction (11) is the fluorine abstraction of hydrogen from diamond surface; reaction (13) is the fluorine adsorption reaction; reaction (12) is the hydrogen abstraction of fluorine from a diamond surface; and reactions (15) and (16) are thermal desorption of hydrogen fluoride and molecular fluorine, respectively, from the diamond surface. Since the molecular desorption rate is small compared to abstraction rates, the thermal desorption reactions (15-17) are neglected. It is important to note that significantly less information is available for the thermal desorption of fluorine from diamond compared with the thermal desorption of hydrogen. Freedman studied the thermal desorption of fluorine from reconstructed diamond surfaces and found that fluorine desorbs across a wide temperature range (300-1200°C).[18,22] In contrast, molecular hydrogen desorbs in a small temperature range of 900 to 1200°C based on extensive thermal desorption studies.[23-28] Neglecting the kinetics of fluorine desorption is therefore not as justified as neglecting the kinetics of hydrogen desorption. However, temperature programmed desorption was used to *measure* the kinetics of thermal desorption of hydrogen from diamond and ultraviolet photoelectron spectroscopy was used to *estimate* the kinetics of fluorine desorption from unreconstructed diamond surfaces. Here, fluorine desorption is seen to occur at temperatures above 800°C, similar to hydrogen desorption. Due to these results, it is permissible to neglect fluorine desorption kinetics in the above reaction set for the purposes of determining the steady state fraction of hydrogen, fluorine, and radical sites on the diamond surface.

Assuming steady state conditions, the net reaction becomes:

$$4H_{gas} + 4F_{gas} \leftrightarrow 2HF_{gas} + F_{2_{gas}} + H_{2_{gas}} \qquad (18)$$

The following rate equations follow from the four abstraction reactions and two adsorption reactions:

$$\frac{dC^H}{dt} = -k_1^f C^H H_g + k_2^f C^* H_g - k_4^f C^H F_g \qquad (19)$$

$$\frac{dC^F}{dt} = -k_3^f C^F H_{gas} + 2k_5^f C^* - k_6^f C^F F_{gas} \qquad (20)$$

$$\frac{dC^*}{dt} = k_1^f C^H H_{gas} - 2k_2^f H_{gas} + k_3^f C^F H_{gas} + k_4^f C^H F_{gas} - 2k_5^f C^* F_{gas} + k_6^f C^F F_{gas}$$

$$C^H + C^F + C^* = C_{Total} \quad (22)$$

The steady state concentration of hydrogen, fluorine, and open-sites on the diamond surface can be calculated by solving this system of equations. Although the hydrogen abstraction of hydrogen (reaction 9), and the hydrogen adsorption reaction kinetics have been estimated (reaction 10), less information is available for the hydrogen abstraction of fluorine or the fluorine abstraction of hydrogen from the diamond surface.

Similar to the case of hydrogen abstraction, these kinetics must be estimated based on analogue gas phase kinetic reactions. The kinetics of the following abstraction reactions are available in the literature:

$$H + CF_4 \leftrightarrow CF_3 + HF \quad (23)$$

$$H + CF_3 \leftrightarrow CF_2 + HF \quad (24)$$

$$H + CF_2 \leftrightarrow CF + HF \quad (25)$$

The kinetics of these three reactions are vastly different. Reaction(23) is very slow, and is given by the following rate expression: $k_f = 7x10^{14} e^{\left(-\frac{43}{RT}\right)}$. Here, the reaction rate is strongly temperature dependent, but slow at any temperature reasonable for diamond growth. At 1300K, the reaction rate is $\approx 40x10^6 s^{-1}$. The kinetics of reactions (24) and (25), however, are very fast compared to reaction (23). These kinetics have been measured at room temperature by Flamm *et al.*, to be the following (for the forward rate constant) $5.5x10^{13} s^{-1}$ and $2.4x10^{13} s^{-1}$ for reactions (24) and (25), respectively. Consequently, radical site fractions will be determined based on the kinetics of reactions (24) and (25).

To approximate the abstraction rate of hydrogen by atomic fluorine, the following gas phase reaction rate was used:

$$F + CH_4 \leftrightarrow CH_3 + HF \qquad k_f = 1.81x10^{14} e^{\left(-\frac{3.97}{RT}\right)}$$

This yields a rate constant of $4x10^{-13} s^{-1}$ at 1300K. Note that this abstraction rate is twice that of hydrogen abstraction of hydrogen. For comparison purposes, the hydrogen abstraction of hydrogen rate constant in the temperature range 300-1200K varies from $1.2x10^9$ $cm^3/mol \cdot sec$ to 1.18×10^{13} $cm^3/mol \cdot sec$ and is therefore extremely temperature dependent.[19] At 300K, the abstraction rate is $217x10^{11} s^{-1}$ which is two orders of magnitude larger than the hydrogen abstraction of hydrogen.

Finally, since the fluorine abstraction of fluorine from the diamond surface is expected to be kinetically slow based on the thermodynamics described in the earlier section of this chapter, its contribution to radical site generation is neglected. The lack of abstraction of fluorine by fluorine results in suppressing the radical site density in the conventional diamond growth temperature range.

The radical site fractions calculated using the fluorine abstraction kinetics of reaction (24) are shown in Figure 8 for three atomic hydrogen to atomic fluorine ratios. In the limit of small fluorine concentration and hence large x, the radical site fraction is the same as in the pure hydrogen system. When fluorine is added, the low temperature radical fraction is significantly increased while the high temperature radical site fraction is depressed. The increase in the radical fraction at low temperatures is due to the enhanced hydrogen abstraction of fluorine and fluorine abstraction of hydrogen in this temperature range. The reduction in radical sites observed at higher temperatures is a consequence of the limited fluorine abstraction of fluorine compared with the hydrogen abstraction of hydrogen (in the pure H_2 system). Although at first glance, studies by Maeda *et al.*, would confirm the deleterious effect of fluorine on the diamond growth rate in the high temperature diamond

growth region, upon further evaluation, they are at best a convolution of gas phase and surface kinetics changes. In Maeda's study, the activation energy for diamond growth measured in the 600-900°C range was increased by successive addition of fluorine to the input carbon precursor mixture (CF_4 vs CF_3H vs CH_4). However, in the experiments, the microwave power was adjusted to affect changes on the surface temperature since no auxiliary means for substrate temperature control was available. Since changing microwave power can very well affect the gas phase kinetics, the measured kinetics were a likely a convolution of the gas phase and surface reactions involved in diamond growth from these precursors mixtures.

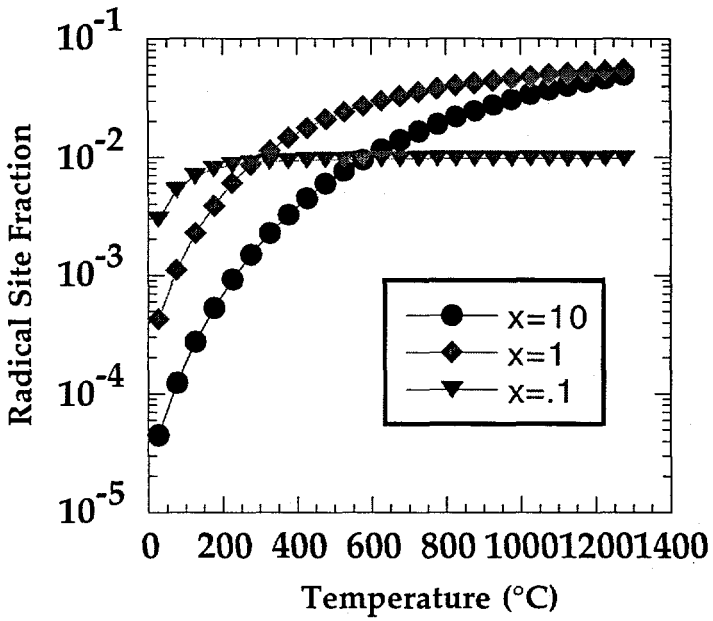

Figure 8 - Radical site fraction in hybrid diamond growth environment of atomic fluorine and atomic hydrogen. The reaction kinetics of the hydrogen abstraction from CF_3 radicals were used in this analysis to approximate the kinetics of hydrogen abstraction of fluorine from the diamond surface. X refers to the ratio of gas phase atomic hydrogen to atomic fluorine.

The large radical site fraction at low temperature range indicates that if the radical site fraction limits diamond growth in the 200-400°C temperature region, then a hybrid diamond growth process using both fluorine and hydrogen could overcome this limitation. However, if both surface diffusion and the radical site fraction limit diamond growth in this region, diamond growth may not be permissible. It is difficult to assess the effects of surface diffusion on the diamond growth rate since the diffusion coefficient of even something as simple as hydrogen is unknown on diamond. However, it is clear that if surface diffusion of the carbon species leading to diamond (such as CH_2 or CH_3) on the diamond surface is limited to the high temperature region, then either the diffusion must be enhanced to achieve low temperature growth or a new diamond growth species must be used. The use of halogens has been suggested as a means of creating new diamond growth species other than the methyl radical, such as CH_2Cl.[13,29,30]

The steady-state radical site fraction (shown in Figure 9) in the hybrid diamond growth environment similar to that of Figure 8 is shown below for the case where the hydrogen abstraction of fluorine from diamond is more correctly approximated by the kinetics of reaction (25). Note that the general trends described in the previous paragraph

are similar except that the depression in the high-temperature radical site fraction is more severe, as would be expected. Again, a x500-x100 enhancement in the low temperature radical fraction is observed suggesting the possibility of enhancement of the low temperature diamond film growth rate.

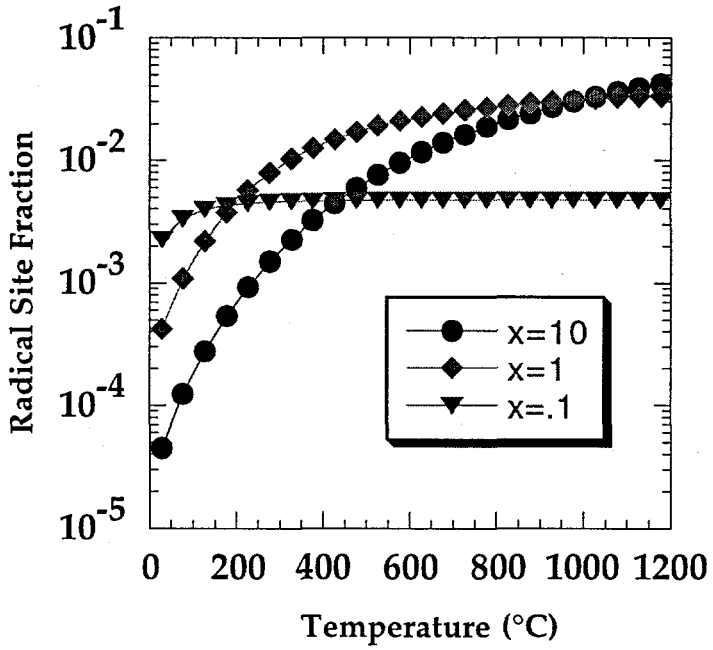

Figure 9 - Steady-state radical site fraction in hybrid diamond growth environment of atomic fluorine and atomic hydrogen. The reaction kinetics of the hydrogen abstraction from CF_2 radicals were used in this analysis to approximate the kinetics of hydrogen abstraction of fluorine from the diamond surface. X refers to the ratio of gas phase atomic hydrogen to atomic fluorine.

The fluorine and hydrogen concentrations are shown in Figure 10 for the radical fractions shown in Figure 8. At low hydrogen concentration, the surface is fluorinated even to 1200°C. It is important to note that the thermal desorption of F_2 and HF were neglected in this calculation and hence, the surface appears fluorinated above the fluorine desorption temperature. However, if a reasonable fluorine flux is present, the thermal desorption of fluorine would still be expected to be slow compared to the hydrogen abstraction of fluorine and the fluorine adsorption of fluorine onto radical sites.

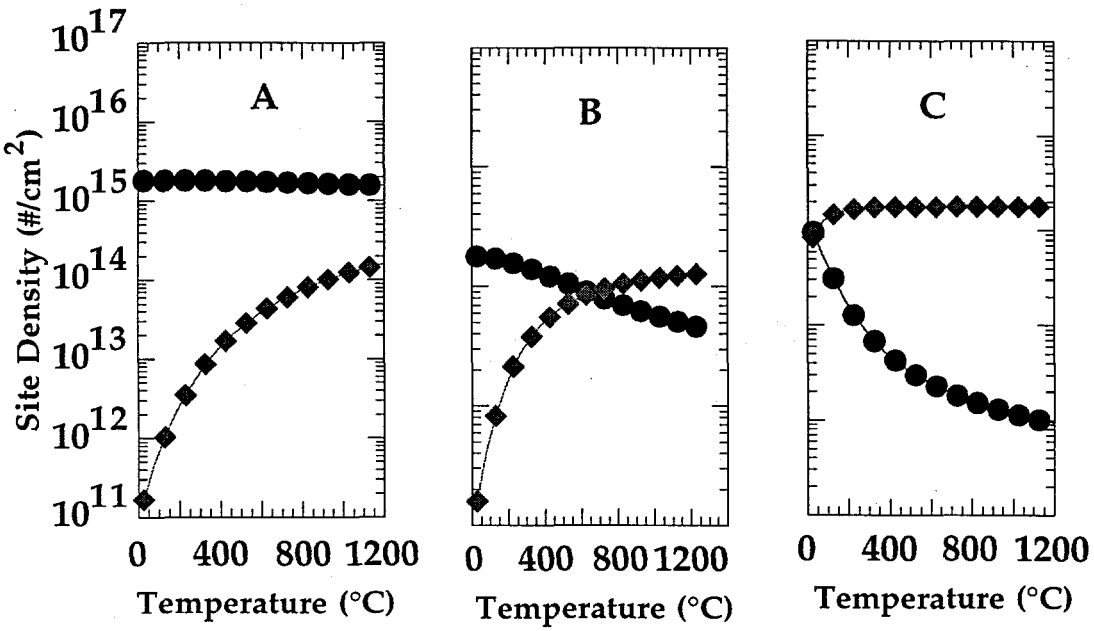

Figure 10 - Hydrogen (circles) and fluorine (diamonds) densities on diamond vs surface temperature for the hybrid atomic hydrogen/atomic fluorine process. The hydrogen to fluorine concentration ratios are A)10, B)1, and C).1.

These calculations suggest the possibility of low temperature diamond growth using atomic fluorine and atomic hydrogen. The enhancement in the low temperature radical site density arises from the enhanced abstraction kinetics of halogen abstraction of hydrogen and hydrogen abstraction of the halogen. In the next section, growth experiments are done to test this hypothesis.

Diamond Growth

Conventional Microwave Plasma System

A microwave plasma reactor was used for the diamond depositions using halogenated precursors. It is important to consider the reasons for using a microwave plasma system. Facilities to handle such hazardous gases as molecular fluorine, molecular chlorine, hydrofluoric acid, and hydrochloric acid were not available and hence, these gases could not be admitted into the process chamber. The limitations on the allowable input gases not only complicated the gas composition measurement using molecular beam mass spectroscopy (MBMS), but in addition, limited the chemistries which could be explored. Therefore, fluorine and chlorine has to be introduced in the form of a stable, fluorocarbon or chlorocarbon precursor. Based on this safety consideration, the following gases were used in this study: CF_4, CH_3F, CH_3Cl, CH_4, and C_2H_2. Although a hot-filament reactor is a viable option for the hydrocarbon input, it is problematic for the fluorocarbons and chlorocarbons for several reasons. In the case of CF_4, thermal dissociation on the hot refractory metal filament (W, Ta at 2000°C) is not expected to be significant due to the carbon-fluorine bond strength. Similarly, the atomic hydrogen dissociation of CF_4 is not expected to be significant due to the limited kinetics of this reaction. In contrast, electron dissociation of CF_4 is known to dissociate CF_4 in both CF_4

and CF_4/O_2 gas discharges. Another significant problem associated with the hot-filament reactor in addition to limited dissociation of CF_4 is the potential degradation in the filament activity in the presence of corrosive gases. Although corrosive gases such as HF and HCl are not directly admitted into the reactor, they may form in the diamond growth process. Degradation of the filament activity in the hydrocarbon system (carbonization), a.k.a. filament poisoning, has been previously observed; this activity loss results in a significantly reduced atomic hydrogen concentration and ultimately, filament replacement.[20] Another compelling reason to use a microwave plasma system is that the MPCVD system is a standard reactor in the diamond community. Therefore, any success using halogenated agents in this reactor can be easily adapted by other researchers in the diamond community.

The microwave plasma system used to deposit the diamond films in this study is shown in Figure 11. The vacuum system consisted of a water-cooled, doubled-walled vacuum chamber; water cooling was used to extract heat injected by the microwave system. In this system, the substrate was mounted upside down using a bayonet-clip mounting apparatus. The bayonet-clip apparatus insured intimate contact between the substrate and the substrate holder. The substrate holder consisted of a diamond-coated molybdenum platform. A tungsten filament was encapsulated in the molybdenum platform to enable resistive substrate heating independent of the microwave power. The diamond-coated molybdenum heater was capable of heating 2" diameter substrates to temperatures in the range of 800-900°C when the microwave plasma was operating. When the discharge was not ignited, the maximum substrate temperature was approximately 800°C. The substrate temperature was measured using a thermocouple (Type K CrAl) spot-welded to the backside of the substrate platform. Optical pyrometer measurements and the thermocouple temperature agreed within 50°C for temperatures above 600°C; however, calibration of the thermocouple reading below 600°C was not possible using the available pyrometer.

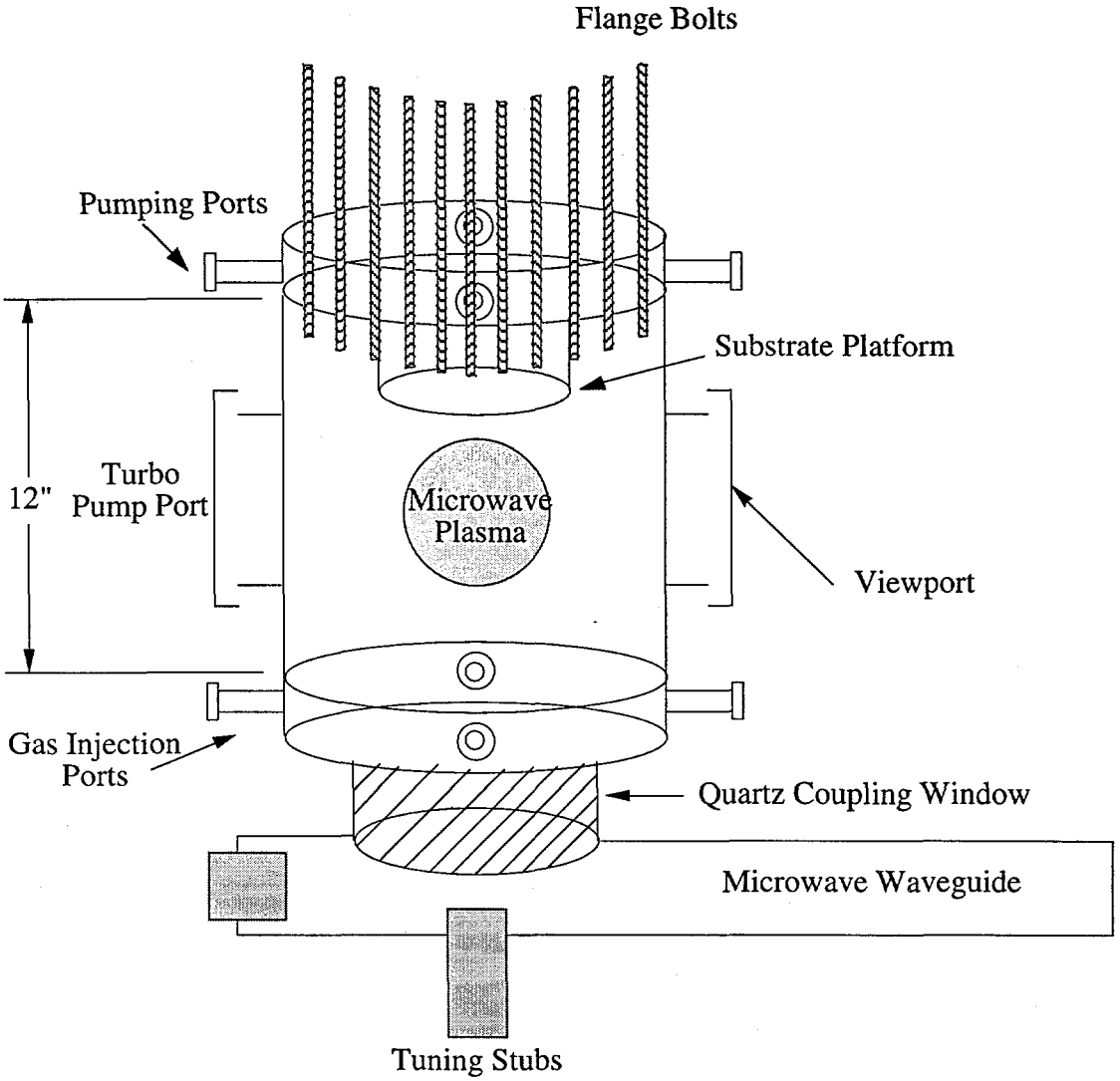

Figure 11 - Schematic of the microwave plasma reactor used to deposit diamond films in this study.

In a separate experiment, the effect of changing substrate temperatures on the local gas density was assessed in the absence of a the microwave discharge. Heating of the substrate was accomplished using the heater encapsulated in the molybdenum platform to raise the temperature up to about 800°C. This local gas density was determined using molecular beam mass spectroscopy (to be described in further detail below). In this experiment, a pure hydrogen mixture was admitted into the reactor chamber at a pressure of 20 Torr. The molecular hydrogen signal intensity (mass 2) was measured as a function of the substrate temperature. Here, the signal intensity was monitored as a function of the substrate temperature for a pure hydrogen mixture at 15 Torr. The reduction in signal intensity as the substrate temperature was raised confirmed the thermocouple measurement; only a change in gas density would change the molecular hydrogen signal intensity at constant pressure and without plasma activation.

To monitor the process chamber pressure during deposition, two baratron pressure gauges were attached to the process chamber via 1/4" stainless steel tubing. Pressures in the .5 to 760 Torr range could be measured using these two baratron heads. In order to maintain the process chamber pressure, the baratron output voltage (via a Type 270B signal

conditioner) was directed into a MKS Type 252A Exhaust Valve Controller. The output of the valve controller was connected to the downstream throttle valve which facilitated pressure control. Prior to all depositions, the process chamber was evacuated to $\approx 5x10^{-6}$ Torr using a turbomolecular pump. Gases were admitted into the process chamber using MKS type 246 mass flow controllers. The deposition system was equipped with two 10 sccm, two 100 sccm, and one 1000 sccm MFC. Since these meters were calibrated for nitrogen in the factory, a calibration for each of the individual gases was done. This procedure involved the following steps: 1) the pressure rise in a calibrated volume was measured as a function of the dial setting; 2) the gas flow rate was determined using the change in pressure with time (dP/dt) and the known calibration volume; and 3) the calculated gas flow rate was plotted as a function of the MFC dial setting. A least squares analysis then yielded the gas flow rate as a function of the MFC dial setting. Typical calibration traces for the 10 sccm CF_4 MFC and the 1000 sccm H_2 MFC are shown in Figure 12.

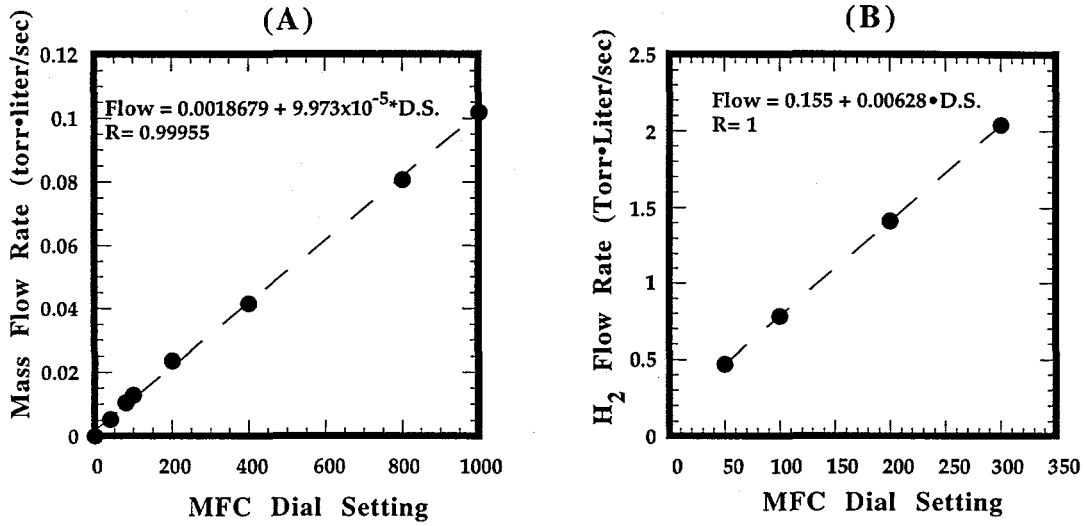

Figure 12 - MFC calibration curves for the A) 10 sccm CF_4 MFC and the 1000 sccm H_2 MFC.

These calibration curves were measured frequently and were repeatable within 5%. The flow controllers were typically operated in the 10-90% of maximum flow range; outside this range, the flow was unstable (particularly for the low flow rate MFC's). When a plasma was sustained in the process chamber, the digital readouts from the MFC's often fluctuated 10-20%; however, the actual gas flow through the MFC's was not fluctuating despite the readout indications. Therefore, all flows in this study were based on these calibration curves and the MFCs' *dial settings*. After exiting the mass flow controllers, the gases were mixed in a mixing bottle and admitted into the process chamber via the ports shown in Figure 11.

Microwave power was injected into the system using an ASTEX™ waveguide and an ASTEX™ S1500i microwave power generator. At typical process pressures of 20-30 Torr, 1000 Watts microwave power, the 8cm-diameter luminous plasma ball would be located just above the substrate surface as is illustrated in Figure 11. To reach the pressure used for depositions (20-30 Torr), the power and pressure had to be raised simultaneously in increments. If the process pressure was too high for a given input microwave power, the plasma ball would relocate to the quartz coupling window and significant amount of power would be reflected back into the microwave power supply. Although this did not harm the window (or the power supply) for short durations, long durations resulted in the

etching of the window and ultimately, its replacement. During a deposition, the reflected power was minimized (typically to 1-10 Watts) using the tuning stubs shown in the diagram. It is important to minimize the reflected power since high reflected powers not only reduce the power coupled into the plasma but, in addition, can damage the microwave power generator magnetron.

Safety considerations at Sandia National Laboratories dictated the gases that could be used in plasma reactor. Since the plasma dissociation of the input fluorocarbon/hydrogen and chlorocarbon/hydrogen gas mixtures could result in hydrofluoric and hydrochloric acid production, the reactor chamber mechanical pump was outfitted for corrosive gases. To this end, crytox oil was used in this mechanical pump (Leybold D80A) and continuously filtered using a Leybold OF1000C Oil Filtering System. The exhaust from the mechanical pump was mixed with copious amounts of molecular nitrogen prior to release into the atmosphere.

When diamond films were grown using fluorinated precursors, additional precautions had to be taken to limit etching of quartz surfaces in the reactor by fluorine-containing species. Hydrofluoric acid, molecular fluorine, and atomic fluorine are all well-known quartz etching agents.[31] To this end, the quartz viewport shown in Figure 11 was coated with magnesium fluoride; this layer significantly reduced the etching of the quartz viewport. In addition, MgF_2 has a low vapor pressure (10^{-8} to 10^{-6} Torr) thereby limiting potential contamination of the film growth process. However, it was not possible to protect the quartz coupling window shown in Figure 11. Quartz etching was not only evident by visual observation of the window, but in addition, SiF_4 was observed in the gas phase when the fluorine concentration was greater than 5-10%.

For all experiments involving halogenated precursor mixtures, polycrystalline molybdenum (Mo) substrates (Aldrich Chemical Co.) were used because molybdenum is relatively impervious to fluorine and hydrofluoric acid (HF); initial experiments indicated that silicon substrates were etched at a faster rate than diamond was deposited thereby complicating subsequent growth rate measurements. The polycrystalline Mo substrates were pretreated by: i) substrate abrading in an ultrasonic agitator for 30 minutes using a mixture of 2 and 40 μm diamond powder and ethanol; and ii) rinsing in deionized water for 5 minutes. Following deposition, the diamond deposit quality was assessed using micro-Raman spectroscopy and the growth rate was determined both by weight change measurements and scanning electron microscopy (SEM) particle size estimates.

In addition to the aforementioned film growth studies to determine the kinetics of diamond growth using halocarbon precursors, the dependence of the diamond film growth rate on the microwave power was assessed for an input gas mixture of $1\%CH_4/H_2$. Scaling of the microwave plasma reactor size to deposit diamond at higher powers and pressures has been one suggested means of reducing the unit costs of diamond deposition. Therefore, it is important to understand the variation in the growth rate for future process development. In addition, measurement of the film growth rate dependence on microwave power for the hydrocarbon system confirms gas composition measurements. These depositions were done on scratched silicon (100) substrates at a substrate temperature of 650°C, $1\%CH_4/H_2$, and 25 Torr chamber pressure. Typical depositions were conducted for 5 hours. Following deposition, the diamond deposit quality was assessed using Raman spectroscopy (laser beam diameter and power were 300 μm and 400 mW, respectively) and the growth rate was determined both by weight change measurements and cross-sectional SEM.

In Figure 13, SEM micrographs are shown of diamond films grown using CF_4/H_2 mixtures. These diamond films were deposited for two hours at 25 Torr, 0.6 carbon mole fraction, 900 watts of microwave power, a total gas flow rate of 400 sccm. It is important to note that the substrate temperature was varied independently of the microwave power,

and hence, the effects of microwave power and substrate temperature were effectively decoupled.

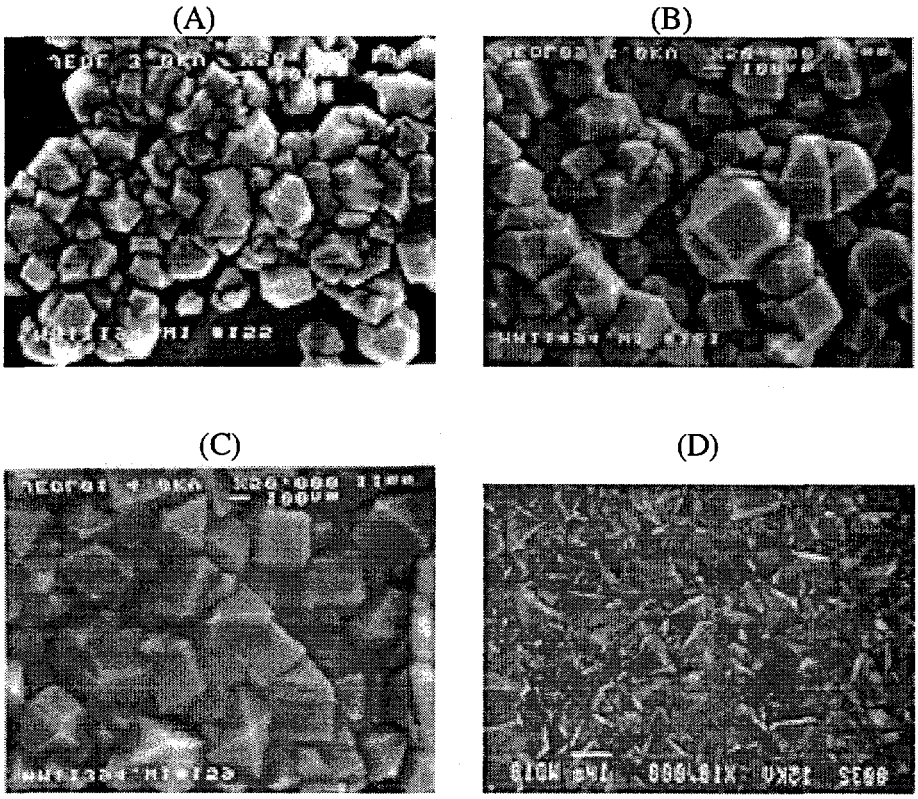

Figure 13 - Diamond films and isolated particles grown using CF_4/H_2 precursors. A) 630°C; B) 700°C; C)740°C; D)850°C Note that the film shown D) was grown for 6 hours whereas the other three films were grown for two hours.

The full films show (111) type faceting for film growth temperatures above 750°C while predominantly (100) faceting is below 750°C. This is typical of diamond films grown using hydrocarbon/hydrogen mixtures. In Figure 14 , SEM micrographs are shown for diamond films grown using CH_3F/H_2 precursor gas mixture. These films were grown using the same carbon mole fraction (.6), microwave power (900 Watts), process pressure (25 Torr), and total gas flow rate. The films and particles shown in Figure 14 were grown at surface temperatures of 620°C, 700°C, and 820°C. In general, the morphologies of the films grown using CH_3F and CF_4 are comparable, with predominantly (100) facets below 700°C and (111) facets above. However, it is important to note that incomplete films can exhibit morphologies which are different from complete films (Figure 13 D). Therefore, regions of the substrate where nuclei coalescence had occurred were used to deduce these type of changes. In the plasma reactor shown in Figure 11, complete coalescence of the films was generally observed in the center region after two hours of deposition, while the outer regions of the wafer exhibited isolated crystallites.

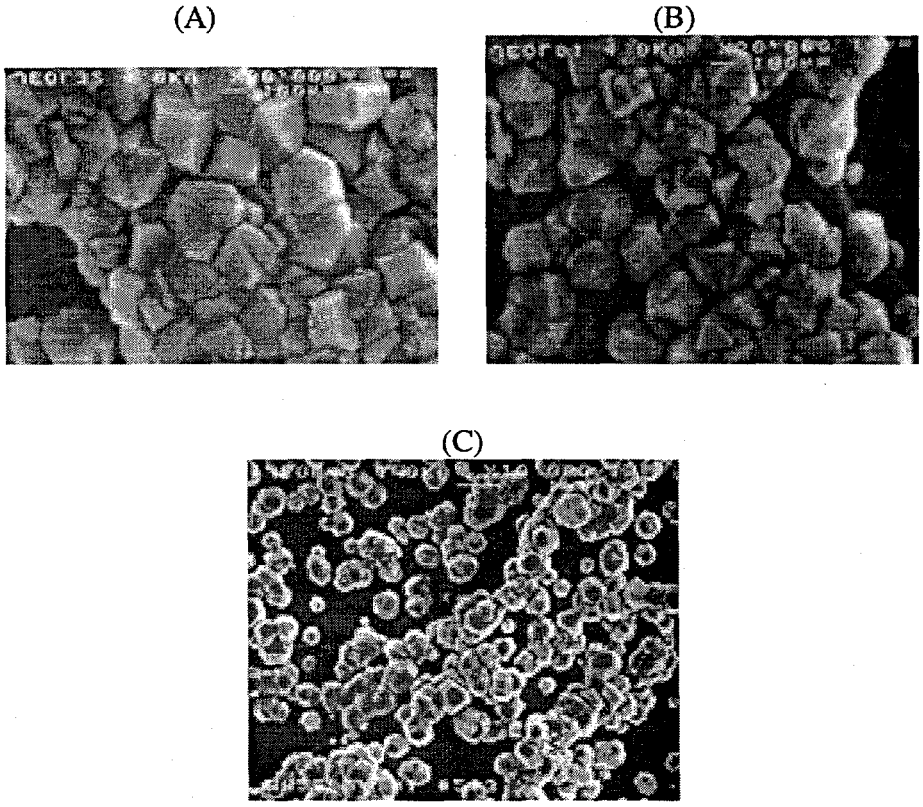

Figure 14 - Diamond films grown using CH_3F/H_2 precursor mixtures with surface temperatures: A)620°C, B)700°C, C)820°C (note magnification is x10000)

In order to determine if the growth kinetics in the fluorocarbon systems are different than the growth kinetics in the hydrocarbon system, measurement of the film growth rate is necessary. There are various techniques which have been used to measure the homoepitaxial diamond film growth rate on diamond single crystals and the diamond film growth rate on dissimilar substrates. For comparison purposes, the most important criterion for a growth rate measurement is that it be conducted the same on all of the samples. To determine the growth rate, three *ex-situ* techniques were considered: cross-sectional SEM, substrate weight change, and particle size estimates using scanning electron microscopy. The thickness of the films can be measured using cross-sectional SEM; this technique is routinely used for substrates which cleave easily (e.g. silicon). However, in this case, preparing a cross-section sample from the 2" molybdenum discs used as substrates in these experiments was not possible. Unfortunately, silicon substrates were etched in the reactor when fluorinated precursors were used, thereby complicating the cross-section measurement. Moreover, due to the short growth time, coalescence of the diamond particles was not observed. Since the cross-sectional SEM measurement was not viable for our substrates, growth rate measurements were done using the weight change of the substrate and the maximum particle size estimated from plane-view SEM's. A comparison of the results of these two techniques is shown in Figure 15. When activation energies for growth are determined based on these two measurement techniques, the resultant activation energies agree within 20%.

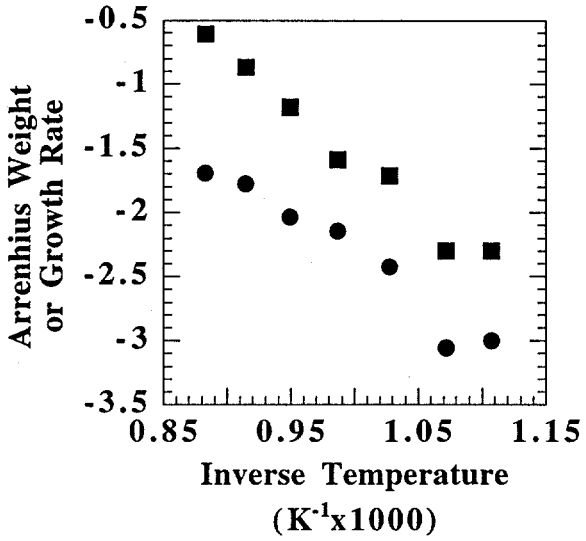

Figure 15 - Arrhenius plot of diamond film growth rate for CF_4/H_2 using particle size estimates from Scanning electron micrographs (squares) and weight change measurements(circles) of the substrate. The activation energies calculated from a least squares analysis were 15.7 and 12.7 kcal/mole for SEM and weight change, respectively.

In order to determine the effect of fluorine additions to the gas phase on the film growth kinetics, activation energies for diamond growth using CF_4/H_2, CH_3F/H_2, and CH_4/H_2 gas mixtures were determined in the temperature range 600-900°C. In Figure 16, the weight change of the molybdenum substrates is plotted in Arrhenius form. The slope of the Arrhenius plot, calculated using a least squares analysis, yields growth activation energies of 12.6±1.8, 13.7±1.2, and 12.4±1.1 kcal/mole, for the CH_4/H_2, CH_3F/H_2, and CF_4/H_2 gas mixtures, respectively. These activation energies agree well with literature reported activation energies (10 kcal/mole-15 kcal/mole)[17,32] for the methane system. Thus, we hypothesize that $CH_3^{\bullet}$ radicals are the principal growth species for both the hydrocarbon and halocarbon gas mixtures.

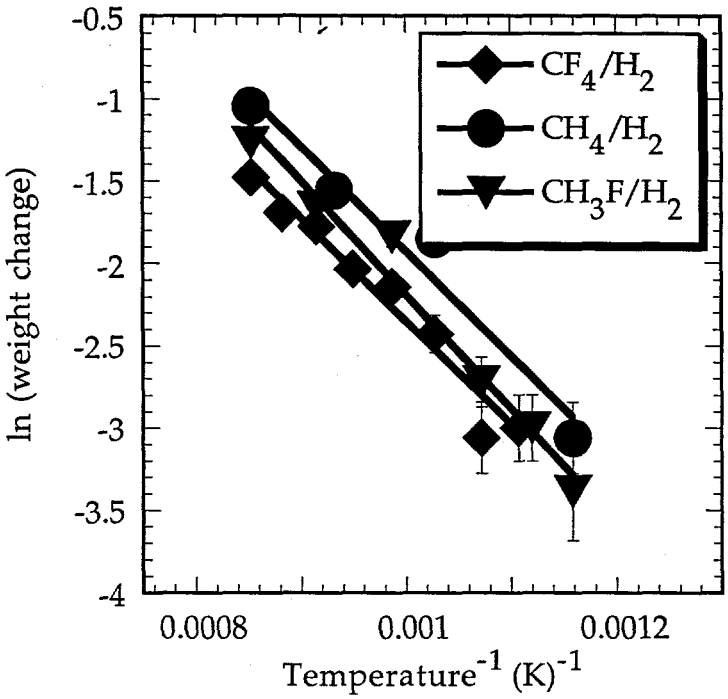

Figure 16 - Arrhenius plot of substrate weight change for CF_4/H_2, CH_3F/H_2, and CH_4/H_2. Note that the slopes of the lines are approximately equal indicating that the activation energy for growth for each mixtures is the same.

The activation energies observed using fluorinated precursors differ from those reported by Maeda.[17] However, the activation energy differences observed by Maeda are related to changes in the $CH_3^{\bullet}$ formation pathways in the gas phase rather than surface reactions involving fluorinated species. In the Maeda study, the substrate was immersed in the plasma and the surface temperature was varied by changing the microwave power. By varying the substrate temperature independently of the microwave power, we separated plasma effects from surface temperature effects. Using molecular beam mass spectroscopy, we have observed that the extent of CF_4 gas phase dissociation in a CF_4/H_2 discharge is dependent on microwave power. The MBMS results are discussed in detail below. Therefore, any variations in film growth rate observed in this study could be attributed to surface phenomena rather than gas phase processes. On the other hand, the changes reported by Maeda are a convolution of surface and gas phase processes.[17]

The variation in crystal habit with surface temperature and gas input mixture, as seen using SEM, further supports that diamond growth proceeds via the same intermediates for the halocarbon and hydrocarbon mixtures. To compare the morphology of the *full* films, six hour depositions were done in the CF_4/H_2 system at temperatures of 650°C and 850°C. Here, we observed that (100) facets were predominant at the 650°C while (111) facets were prevalent at the 850°C. Such variations have been previously observed by other researchers for hydrocarbon mixtures. Similarly, Maeda observed that variations in crystal morphology were similar for both hydrocarbon and fluorocarbon gas sources.[17] The fact that the morphology was independent of precursor suggests that diamond growth occurs via similar reaction pathways.

These experimental results are also consistent with studies by McMaster, *et al.*, and Mitomo, *et al.*, who demonstrated that the film growth rates in MPCVD were independent

of the carbon precursor (C_2H_2/H_2, C_2H_4/H_2, and CH_4/H_2) provided the carbon to hydrogen ratio, pressure, and microwave power were constant.[33,34] Moreover, although surface temperature changes can significantly alter film growth rate and morphology, they do not effect the gas phase composition.[33] Hence, the activation energies measured in our study are independent of the gas composition. Finally, the observation that the film growth rate is independent of the carbon inlet identity is consistent with Bai who found no preference for fluorine-based diamond growth using isotopic labeling.[35]

The lack of atomic fluorine incorporation into the film during deposition provides further support for the hypothesis that diamond growth proceeds via the same radicals for the halocarbon and hydrocarbon mixtures. An XPS spectra is shown in Figure 17 following a two hour deposition using 0.6% CH_3F/H_2 at 660°C. The amount of fluorine detected was estimated to be approximately 1% of the near surface region composition (probing depth ≈ 60 Å). Note that a small amount of tin contamination was also present which we attributed to impurities in the molybdenum substrate. Since the diamond deposit was not a full film, molybdenum was detected in addition to carbon. The aforementioned film was then subjected to argon ion sputtering for ten minutes at using 5000 volt argon ions. Although trace amounts of fluorine were detected following deposition, no fluorine was detected after argon ion sputtering (Figure 18). The lack of fluorine incorporation into the film is consistent with molecular beam gas composition measurements in the CF_4/H_2 system where undissociated CF_4 and HF were the only fluorinated species present near the surface during film growth. Fluorine incorporation into the diamond film is not expected with negligible concentrations of fluorine atoms or CF_x (x=1-3) radicals in the gas phase.

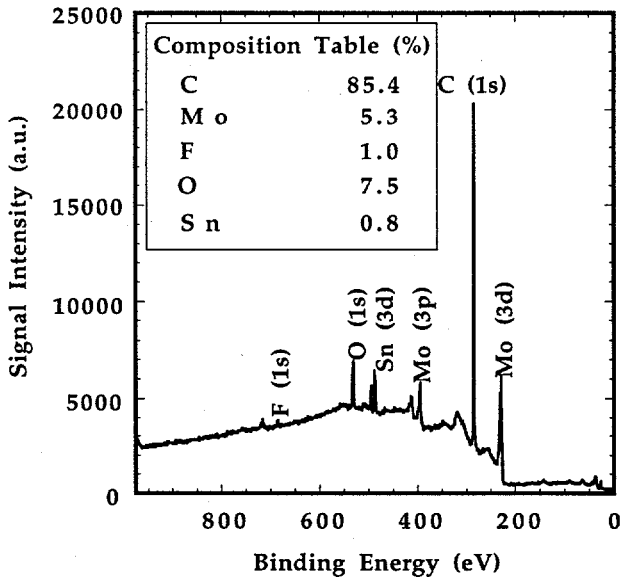

Figure 17 - XPS spectra following growth and air-transfer.

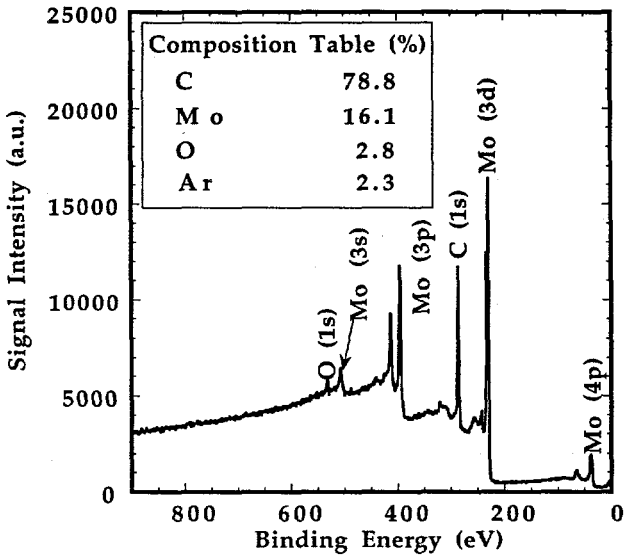

Figure 18 - XPS spectra following argon-ion sputtering which shows limited incorporation of fluorine into diamond film.

Near-surface Gas Composition Characterization

Using molecular beam mass spectroscopy, the radical and stable species absolute mole fractions were measured for CH_4/H_2, CH_3F/H_2, CF_4/H_2, and CH_3Cl/H_2 precursor mixtures in the conventional microwave plasma system. For the CF_4/H_2 mixtures, hydrofluoric acid and carbon tetrafluoride were the only fluorinated species observed; additionally, neither F-atoms or CF_x (x=1-3) radicals were detected near the substrate surface. The abundance of HF in the fluorocarbon/hydrogen plasmas, near the substrate surface, indicates that the input fluorine is consumed by homogenous gas phase reactions, and hence, is not transported to the surface. For the CH_3Cl/H_2 mixture, HCl was found to be the only chlorinated species present near the substrate surface during growth. In both systems, the dissociation of HF and HCl is not strong by the plasma; therefore, significant atomic species concentrations are not observed. For both systems, the methane and methyl mole fractions track, and the hydrogen abstraction reactions determine the ultimate hydrocarbons species present near the substrate surface.

The principle gas phase species detected near the substrate surface during diamond synthesis from a $CH_3F/H_2/Xe$ input mixture were the following: HF, C_2H_2, CH_4, CH_3, H, and C_2H_4. Signals originating from SiF_4 were also measured when the input mole fraction of fluorine was greater than .04. This etching was not due to etching of silicon substrates because substrates were not used during the gas composition measurements. The etching is possibly due to etching of the quartz coupling window or etching of a viewport used to visually monitor the plasma. Most likely, SiF_4 originates from the quartz coupling window because the viewport was coated with magnesium fluoride to inhibit etching. In figure 19, the mole fractions of these principle constituents are shown as a function of the input methyl fluoride concentration for the following deposition conditions: 25 Torr, 900 Watts microwave power, a total gas flow rate of 100 sccm, and a surface temperature of 650°C. Note that in all cases, there was an approximate two order of magnitude increase in the acetylene mole fraction while the atomic hydrogen concentration remains nearly constant.

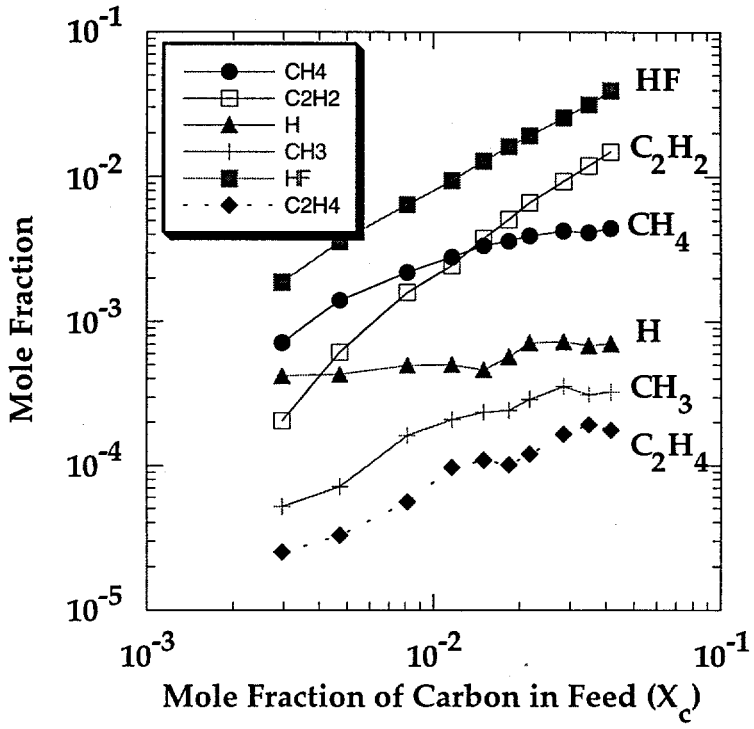

Figure 19 - Gas composition as a function of the inlet CH_3F mole fraction for $CH_3F/H_2/Xe$ mixtures. Note that all the input fluorine was converted to hydrofluoric acid by the plasma.

It is important to note that the methyl radical and atomic hydrogen mole fractions are quantitatively similar to the hydrocarbon system, indicating that not only would the surface temperature dependence of the growth rate be similar, but in addition, the *absolute* growth rates should be similar. Therefore, the activation energies measured for diamond growth in the conventional microwave plasma system are consistent with a diamond growth mechanism from methyl radicals and atomic hydrogen.

The gas composition was also measured at surface temperatures of 650°C, 750°C, and 800°C while the process pressure was maintained (see Figure 20) for both CH_4/H_2 and CH_3F/H_2. The radical species mole fractions were independent of the surface temperature, similar to the case for hydrocarbon system discussed in the previous section.

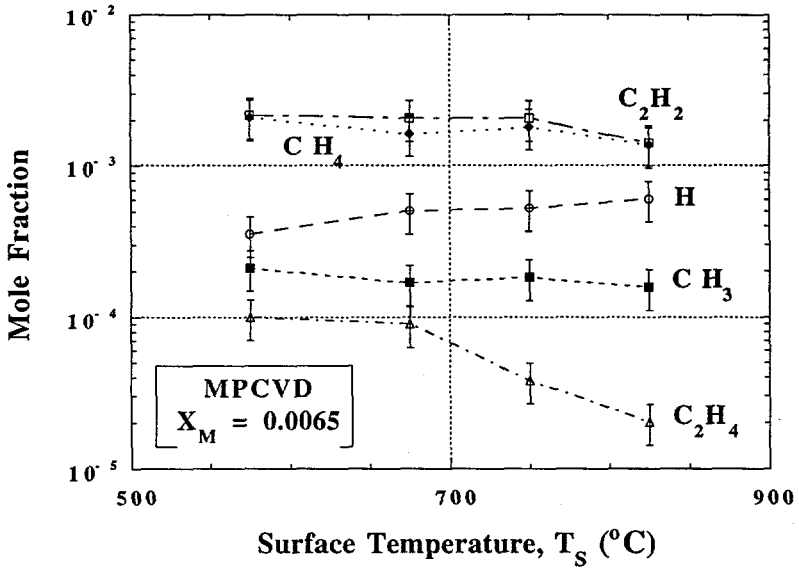

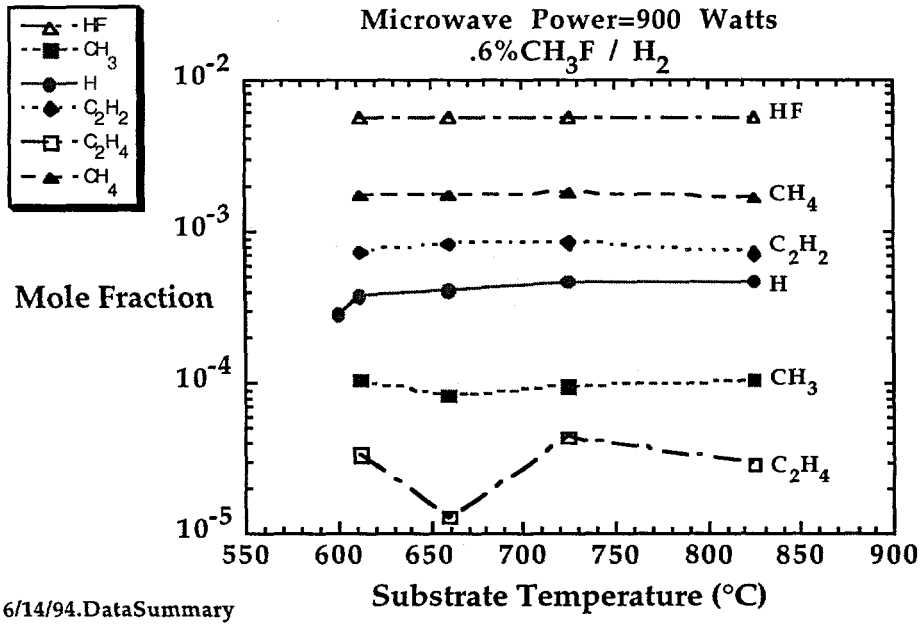

Figure 20 - Gas composition as a function of surface temperature. A. CH_4/H_2 system. B. CH_3F/H_2 system.

The mole fractions of C_2H_2, CH_4, CF_4, HF, C_2H_4, H, and CH_3 are shown in Figure 21 as a function of microwave power. The H_2 flow rate was 398 sccm, the CF_4 flow rate was 2.42 sccm, and the Xe flow rate was 5.87 sccm. As the power was increased, CF_4 dissociation increased and therefore, the hydrocarbon concentrations increased. CH_3 increased by a factor of 5 while acetylene increased by a factor of 10. The

increased dissociation of CF_4 indicates that the primary process to CF_4 dissociation is electronic. However, increase in the electron density which causes CF_4 dissociation to increase does not significantly increase the dissociation of molecular hydrogen; this mole fraction of atomic hydrogen is relatively independent of the microwave power within the experimental error of the measurement. The decrease in the H/CH_3 ratio as the microwave power increased suggests that the diamond film growth rate would increase with increasing microwave power. However, only HF and CF_4 were observed as the microwave power is raised, so therefore the temperature dependence of the growth rate would be similar for the hydrocarbon based diamond CVD. These results are consistent with the hypothesis that Maeda's activation energies for diamond growth were a convolution of gas phase and surface kinetics.

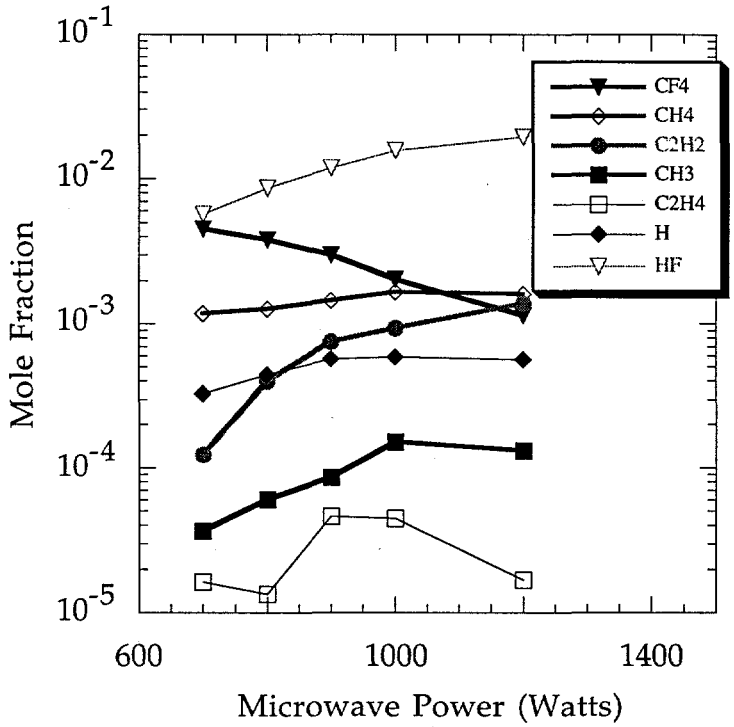

Figure 21 - Gas composition using $CF_4/H_2/Xe$ gas mixture measured at a surface temperature of 650°C, 25 Torr, and a carbon mole fraction of 0.6. Note that the hydrocarbon content significantly increases as the plasma dissociation of CF_4 is increased.

In summary, neither atomic fluorine nor carbon-fluorine radicals were observed in the near surface region when fluorine was introduced into the gas phase during diamond growth (in the form of CH_3F and/or CF_4). If the carbon mole fraction is constant, the microwave power constant, the growth processes for the CF_4/H_2 system and the CH_4/H_2 system are the same; specifically, the diamond film is grown using CH_3 radicals and atomic hydrogen. The fact the CH_3 mole fraction increases with increasing microwave power indicates that the growth rate should increase, as has been observed for the CF_4 system wherein both microwave power and substrate temperature were changed. For the CH_4/H_2 plasma, this is not expected. Both the diamond growth studies described in the previous section and the gas composition measurements of this section demonstrate the lack of halogen transport to the diamond surface during growth. Rather, the halogen reacts with

atomic hydrogen to form either HF or HCl. Normal diamond growth from methyl radicals and atomic hydrogen is not altered by either of these very stable gases.

In order to transport atomic hydrogen and atomic fluorine to the growth surface simultaneously during growth, significant changes must be made. To this end, two diamond growth systems were developed to facilitate halogen transport to the diamond surface. In a flow tube system, gas flow rates were maximized in order to minimize gas phase reactions during diamond growth. In the other system, atomic hydrogen and atomic fluorine were generated in isolated chemical environments.

The flow tube system is shown schematically in figure 22a. This apparatus consisted of a quartz flow tube of outer diameter .5" with a center tube of diamond 1/8". The substrate heater was placed directly below the center tube exit; note that the substrate temperature was independent of the microwave discharge parameters since it was located downstream of the microwave discharge. For conventional diamond growth, H_2 was metered into the outer tube while methane was admitted into the small tube. A microwave discharge (Evenson cavity) was used to generate a discharge in the outer tube in order to create atomic hydrogen. At the tube exit, atomic hydrogen reacts with methane to form methyl radicals; both radical species are then transported to the diamond surface. At a pressure of 20 Torr, and with the substrate located directly underneath the center tube, diamond films were grown. As the distance between the center tube and the substrate was raised, diamond growth was inhibited. The strong sensitivity of diamond growth rate was due to the precipitous loss of either methyl and/or atomic hydrogen at the tube exit.

To generate atomic fluorine in this environment, a *pulsed* diamond growth process was envisioned wherein a CF_4/O_2 plasma (CF_4/O_2 through outer tube) generates atomic fluorine in the first pulse and a CH_4/H_2 plasma (CH_4 center tube, H_2 outer tube) generates methyl radicals and atomic hydrogen in the second pulse (see Figure 22b which shows side injection of CH_4/H_2). In principle, the atomic fluorine to atomic hydrogen ratio can be varied as a function of surface temperature in order to validate the previously described model.

Unfortunately, diamond growth using this pulsed gas technique was not successful. Based on molecular beam mass spectroscopy gas composition analysis of the flow tube system, appreciable atomic fluorine concentrations were only produced at low pressures (in the .5 Torr range). Diamond growth in this pressure range is extremely slow due to reduced radical species flux. Therefore, the conditions which optimized halogen transport to the diamond surface were not conducive to diamond growth. In addition, approximately 10-30 % O_2 maximized the fluorine flux but also lead to atomic oxygen production; atomic oxygen is known to etch carbon and could complicate the interpretation of diamond growth rates. Use of CF_4/H_2 plasma instead of CF_4/O_2 was also investigated as a means of generating atomic fluorine and/or carbon-fluorine radicals. Similar to CF_4/O_2, measurable CF_3 and CF_2 concentrations were only observed at low pressures; as the pressure was raised (above 1 Torr), recombination reactions resulted in CF_4 formation.

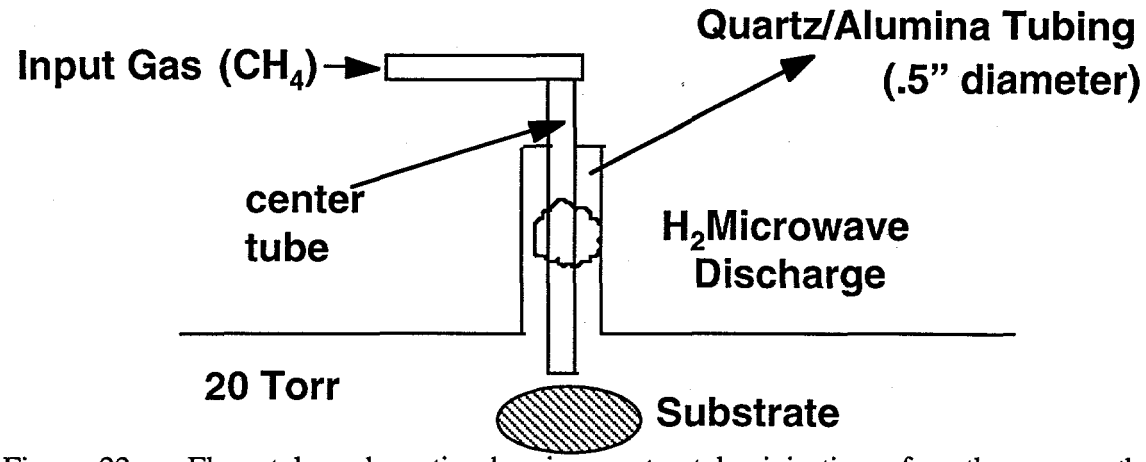

Figure 22a - Flow tube schematic showing center tube injection of methane near the substrate surface. Note atomic hydrogen is generated in the outer tube in a remote microwave discharge.

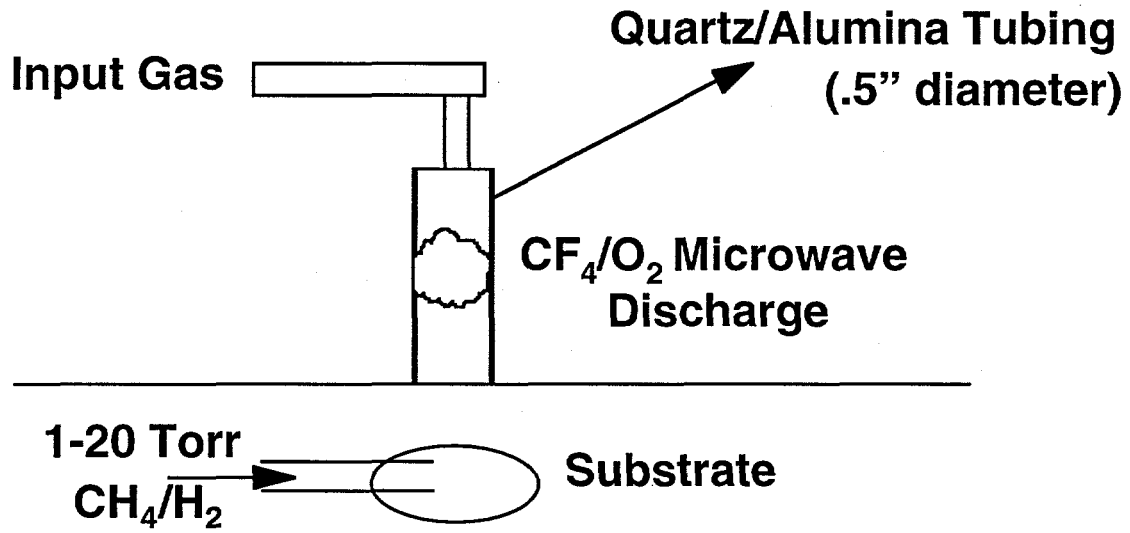

Figure 22b - Flow tube system for diamond growth. Note that here, CH_4/H_2 injection is shown from a side tube.

Diamond growth using atomic fluorine was attempted in a system which isolates the chemical environments of each radical species. This system was been previously used to grow diamond from atomic hydrogen and atomic carbon and is shown schematically in Figure 23.[36] Here, atomic hydrogen is generated by a hot filament in an isolated chemical environment while atomic carbon is generated by sputtering carbon from a graphite target. Chemical isolation is achieved by rotating a substrate plate over each emitter with the plate to emitter distance minimized (≈200μm). In addition, high gas flow rates in the emitters minimized cross-talk between adjacent emitters. To add fluorine to sequential diamond growth, a third emitter was added which consisted of a CF_4 discharge or an SF_6 discharge. This is shown schematically in Figure 23 as "F." Similar to the atomic carbon source, helium was used as a diluent and a molybdenum target was used as a target material. Preliminary investigations showed that diamond was deposited at a higher growth rate with a different morphology in the C/F/H rotation sequence (SF_6 used as F source) vs the conventional C/H sequence. Unfortunately, further testing in this reactor was complicated

by the presence of surfaces not amenable for atomic fluorine and/or hydrofluoric acid exposure. Moreover, measurement of the atomic fluorine flux to the surface was not possible in this reactor thereby complicating interpretation of the film deposition results. Consequently, a complete redesign of this reactor would have been necessary.

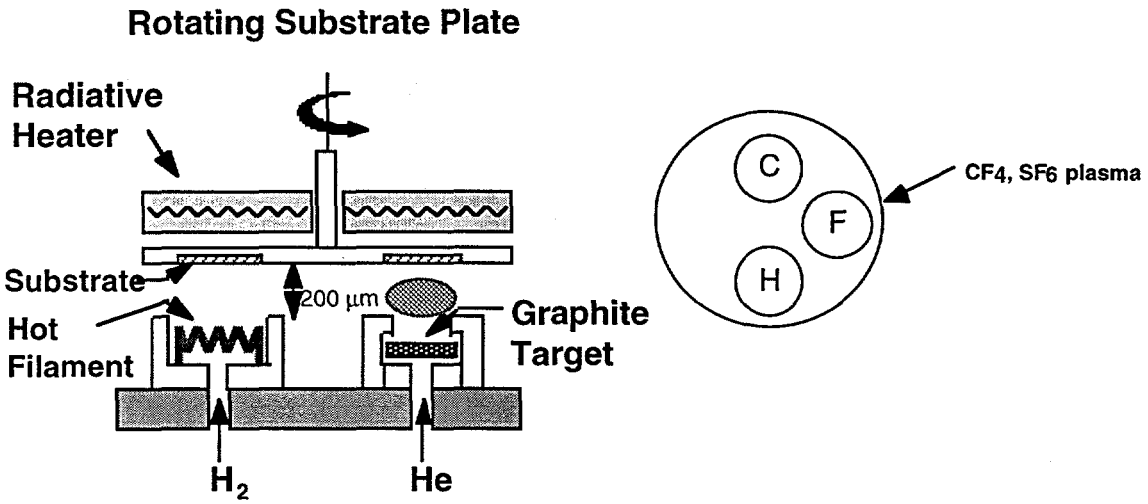

Figure 23 - Sequential Reactor schematic. Conventional diamond growth in sequential reactor is accomplished using C-H sequence; here, addition of an F step in the process was tested.

In summary, atomic fluorine transport to the diamond surface was limited in a conventional microwave plasma reactor due to gas phase reactions. In non-conventional reactors, atomic fluorine transport was similarly complicated. Therefore, future work must involve developing improved methods of transporting atomic fluorine to the diamond surface. Modification of the sequential reactor (in terms of materials compatible with fluorine) is a viable alternative but was not pursued in this study. The goal of testing the model previously described therefore remains elusive.

Although fluorine transport to the diamond surface during growth proved to be limited by the diamond reactor, *ex-situ* fluorination of diamond surfaces using plasma reactors was viable. Here, air-stable fluorinated surfaces could be prepared by replacement of atomic hydrogen on the surfaces with atomic fluorine (fluorine abstraction of atomic hydrogen). The use of fluorinated diamond surfaces as a means of preparing air stable, thermally stable field emission cathodes is described in the next section.

FLUORINATION OF DIAMOND SURFACES

Introduction

The fluorination of diamond (and/or carbon surfaces) has received attention recently due to the reported use of fluorine in diamond growth (see Introduction) and the potential reduction of the diamond friction coefficient. Due to fluorine's relatively small size (an atomic radius approximately twice that of hydrogen), large coverages of fluorine may be achievable on diamond surfaces. Moreover, fluorine might be an extremely stable passivation layer. What is much less clear is any potential improvement in the electron emission characteristics of diamond surfaces using fluorine. Upon initial inspection,

fluorine would not be expected to improve the electron emission characteristics of diamond surfaces. Although substantial coverages of fluorine might be realizable on diamond surfaces, fluorine's extreme electronegativity would only serve to raise the diamond surface electron affinity. Since fluorine is extremely electronegative, the work function of a fluorinated diamond surface should be larger than the work function of a hydrogenated diamond surface. Using photoemission, the electron affinities of hydrogenated, fluorinated, and bare diamond surfaces were measured. As expected, the electron affinity of the fluorinated surface was the largest for both single crystals and chemically-vapor deposited films. However, fluorine acts to enhance the reactivity of diamond surfaces to cesium rather than directly participating in the field emission process.

Cesiation is a possible means of lowering the work function of diamond and diamond-like-carbon materials thereby reducing the critical threshold field. The cesiation of surfaces to produce the NEA condition is a well-known process in GaAs photocathodes. Typically, NEA photocathodes are produced using heavily doped p-type material. Pickett recently predicted that the cesiation of an oxygenated diamond surface can even effect the NEA condition.[37] In addition, such an overlayer on the diamond surface was predicted to be chemically stable. Experimentally, field emission from cesiated diamond surfaces has recently been reported by Geis *et al.*[38] Although experiments were not done to assess the NEA of these diamond surfaces, cesiation of the oxygen diamond surface yielded a field emission material with the low turn on voltage and high chemical stability. In Geis's study, treatment of B-, Li-, P-, and N- doped diamond crystals in an oxygen plasma, cesiated, annealed, and exposed to air exhibited enhanced electron emission for all the crystals except the boron-doped. In fact, emission at fields as low as .2 V/μm was observed for the nitrogen-doped diamond. In these studies, the Cs-O surface structure lowers the work function thereby enhancing the field emission behavior. The enhancement of the secondary electron yield of CVD diamond films by deposition of CsI was reported by Mearini *et al.*[39,40] Here, CsI was deposited onto diamond surfaces which were subsequently exposed to an electron beam; the authors argued that the electron beam effect the dissociation of CsI thereby desorbing iodine while leaving cesium bonded to the diamond surface. This cathode was stable in air (recoverable) and up to annealing temperatures of 120°C. Carbon surfaces that have been cesiated using an intermediate fluorination step have air stable and thermally stable field emission characteristics.

Experiment Description

Type IIB semiconducting diamond crystals were obtained from Doubledee Harris. Type IIB diamonds are lightly boron doped and therefore have some conductivity at room temperature. Four-point probe measurements made at room temperature indicated a dopant concentration of $\approx 10^{16}$ to $10^{17}/cm^3$. Photoemission measurements where conducted at room temperature where a limited amount of the boron acceptors were ionized. However, these single crystals were conductive enough that significant charging was not detected. There were two options considered for hydrogenating the diamond single crystals: polishing in .25μm diamond grit/methanol solution and immersion in a hydrogen plasma. Although the fine polish was initially done on the single crystals to remove coarse polishing damage done by the diamond distributor, the hydrogen plasma treatment was used to hydrogenate the diamond surface.

Hydrogen treatment of the diamond crystal involved immersion of the crystal into a hydrogen microwave plasma. The hydrogen plasma was formed in an ASTEX™ 5 kW reactor with a water-cooled substrate stage whereas the deposition chamber used for the growth experiments was an ASTEX™ 1.5 kW reactor with a substrate heater. This chamber is largely similar to the deposition chamber described in the growth section of this report, with the exception of the higher power and substrate cooling capabilities. In the

high power chamber, the diamond crystals were placed on a molybdenum holder which was in direct contact with the water-cooled substrate stage. During the plasma treatment, the diamond crystal was positioned 1-2 cm below the luminescent microwave plasma ball. The hydrogen treatment parameters were 3 hours, 750 Watts, 15 Torr, and pure hydrogen gas. Under these conditions, the substrate temperature is expected to be below 300°C, although we were unable to measure this surface temperature precisely.

Plasma fluorination of the hydrogenated diamond surfaces was done using an Ion and Plasma Equipment RIE 1000TP reactor. This reactor consisted of a capacitively coupled RF discharge with water-cooled electrodes. The diamond crystals were placed directly on the substrate electrode and the chamber was evacuated to a pressure less than $1x10^{-6}$ Torr prior to plasma ignition. When the base pressure was reached, SF_6 was admitted into the chamber until a pressure of 20 mtorr was reached. Pressure was measured downstream of the reactor chamber using a baratron gauge. Note that the reactor chamber was pumped by a corrosive-gas turbo pump during the plasma exposure. When the process pressure was stabilized, the RF plasma was ignited; typical plasma parameters for the fluorine exposure done in this study were 50-60 Watts and -70 self bias. Since the substrate was located on a water-cooled electrode, it's temperature was maintained below 200°C during the short plasma exposure.

It is important to note that plasma fluorination of diamond surfaces lead to increased stability of fluorine on the diamond surfaces. Previous reports of fluorination of bare diamond surfaces by exposure to atomic fluorine beams has shown that fluorine desorbs continously over the temperature range of 300-1000°C.[18,22,41] In contrast, fluorine desorption from plasma-fluorinated surfaces occurs in the temperature range of 600-1000°C. Valence band and survey scans are shown in Figure 24. Here, a fluorinated CVD diamond surface was annealed to a given temperature and cooled to room temperature where the photoemission spectra was measured (details described below). Note the area under the F(2p) peak is unchanged until temperatures >600°C area reached. The mechanism for the enhanced thermal stability is not known but is postulated to be related to the surface structure of the fluorinated diamond surface. This surface structure is 1x1 rather than the reconstructed 2x1 surfaces achieved by atomic fluorine beam fluorination of bare diamond surfaces.

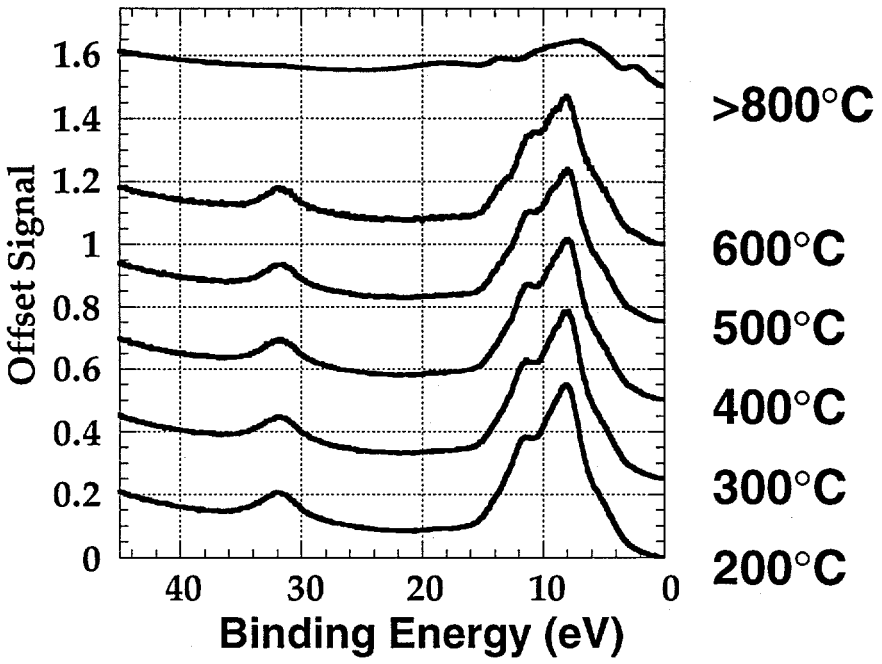

Figure 24 - UPS spectra of fluorinated CVD diamond surface following annealing to temperatures shown on right. The F(2s) peak is observed at a binding energy of approximately 32 eV.

Following the plasma treatments, ultraviolet photoemission (UPS) measurements were done at the Stanford Synchrotron Radiation Laboratory using beam lines 8-1 and 1-2. The photon energy for both these beam lines was limited to be less than 200 eV. Consequently, it was not possible to measure the carbon core level using the UPS apparatus. However, cesium core levels (4d and 5p) and fluorine core levels (2s and 2p) were measurable, in addition to the valence band. Valence band measurements were done using a photon energy of 80eV while cesium 4d core level spectra were collected using a photon energy of 130 eV. Photoelectrons were detected using a cylindrical mirror analyzer (CMA) whose focus was at the position of the sample. Note that the collection angle for the CMA, based on the geometric relationship between the sample and the CMA, was 45°±5°. Since measurements of the carbon core level were not possible using the UPS apparatus, the diamond crystals were transferred to a separate UHV chamber equipped with an AlKα xray source. In this way, both wide survey scans and high resolution carbon scans could be done. Note that transfers between the high vacuum analysis chambers and the plasma chambers were all done in air.

The electron affinity characterization of diamond surfaces required measurement of the electron energy distribution curves (EDC). Here, the diamond crystal holder was biased either -10 volts or -20 volts while the crystal was exposed to the synchrotron radiation. Most of the EDC measurements were done using a photon energy of 80 eV and a bias potential of -10 volts. The EDC was extremely sensitive to the bias potential but not as sensitive to the photon energy (in the range 10-80 eV). The EDC's dependence on bias voltage was most likely due to an electron focusing effect. Measurement of the EDC and VB were critical for extracting the electron affinity of diamond surfaces and calculated the band bending region width.

The effect of cesium deposition on the photoelectron emission from diamond surfaces was analyzed by depositing cesium on the surfaces in the UPS chamber using a SAES cesium dispenser. The SEAS cesium dispenser involves annealing of a cesium containing compound to the point where the compound is broken apart. A getter material in the dispenser is used to collect the other element formed upon compound breakup while the cesium is directed toward the diamond sample. During cesiation, the diamond crystal was rotated within line-of-sight of the diamond crystal. No attempt was made to measure the cesium deposition rate during a cesium exposure. Cesium was deposited on all surfaces within line-of-sight of the cesium dispenser, including other sample holder surfaces. This severely impacted measurement of the EDC and VB of the diamond single crystals due to their small size relative to the molybdenum sample holder. Measurement of the EDC for crystals directly mounted on the sample holder yielded contributions from both the diamond crystal and the sample holder. This was not problematic for the CVD diamond films grown directly on the Mo sample holder or diamond films grown on silicon (due to the large sample size). To eliminate the sample holder contribution for the case of the single crystals, the diamond crystals were mounted .5-1 cm above the Mo base plate using a Ta clip apparatus. By changing the electron focus depth (with respect to the CMA), the contribution of the sample holder was effectively eliminated. Cesium depositions on only the holder materials (Mo, Ta) were done to confirm this result.

Cesiation of Hydrogenated Diamond Surfaces

The electron energy distribution curve and the valence band spectra for the hydrogenated C(110) surface following cesiation are shown in Figures 25 and 26. Here, using a procedure detailed by Pate et al.,[3] the electron affinity was estimated to be 0 eV. This hydrogenated surface was nearly or partially NEA after the hydrogen plasma treatment and clearly had the lowest work function of the diamond surfaces prior to cesium treatment. The particular features in the valence band, and their respective positions (to valence band maximum) are consistent with literature reported results. Following cesiation, this surface exhibited a drastically enhanced NEA feature measured under collection conditions similar to the spectra shown in Figure 26 (e.g. V=-10). However, the light intensity was reduced significantly due to saturation of the electron multiplier. Although cesium dramatically influenced the NEA condition, few changes except a shift were observed in the valence band spectra. This shift corresponds to 0.4 eV and has been previously attributed to increased downwards band bending. The NEA was estimated to be -0.5 eV based on the spectra shown in Figure 26. Saturation cesium coverage was reached after 15 minutes as shown in Figure 27 and was estimated to be 0.1 monolayers based on similar measurements in the GaAs system. It is clear that a small amount of cesium on the hydrogenated diamond surface dramatically enhanced the NEA condition without changing the valence band structure.

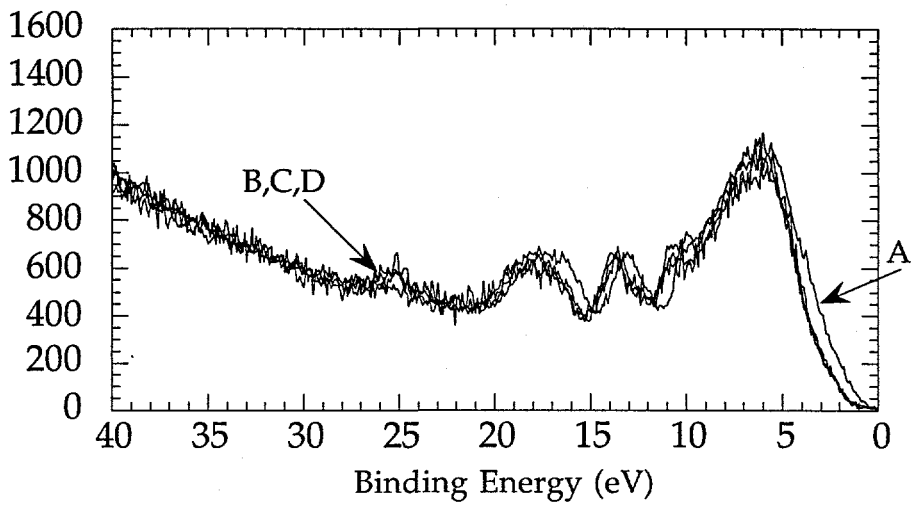

Figure 25 - VB spectrum following cesium deposition to saturation on the hydrogenated C(110) surface. A) installed; B) 15 minutes; C)30 minutes; D)40 minutes.

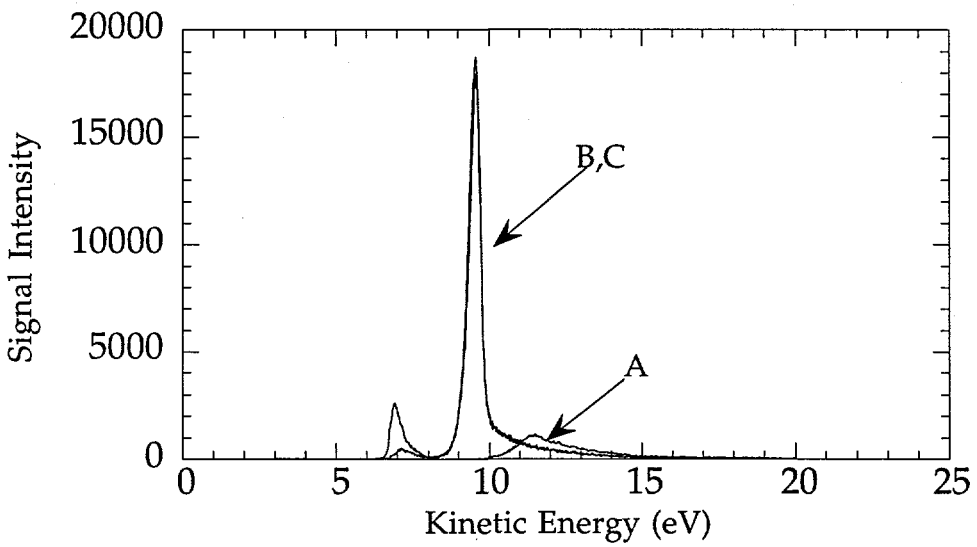

Figure 26 - EDC following cesium deposition to saturation on the C(110) surface. Note the strong enhancement in the NEA feature following cesiation. A) installation and 600°C anneal; B) 15 minutes cesium deposition; and C) 30 minutes cesium deposition.

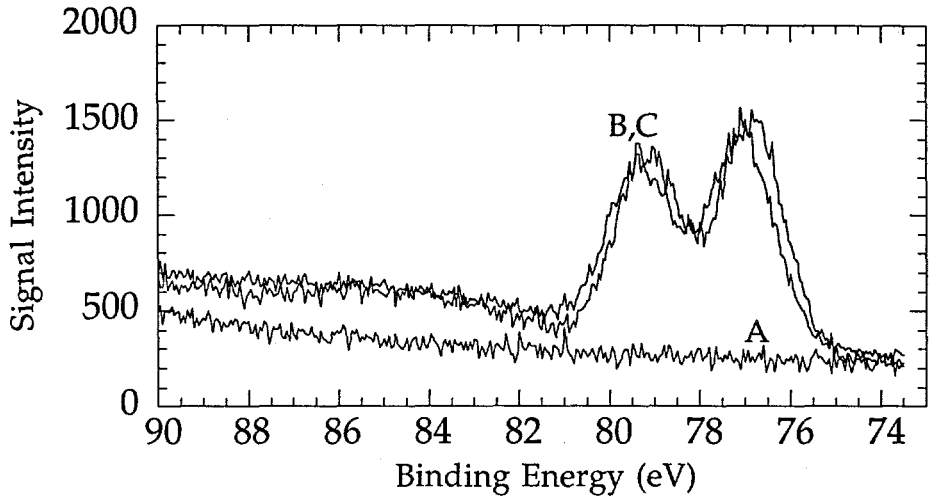

Figure 27 - Cs (4d) spectra following cesium deposition to saturation on the C(110) surface. Note the small coverage obtained even at cesium saturation.

Cesiation of Fluorinated Diamond Surfaces

The electron affinity of the fluorinated surface was at least 3 eV higher than the hydrogenated surface. This is consistent with the large electronegativity of fluorine. The VB spectra and cesium core level spectra are shown in Figures 28 and 30, respectively, following cesium deposition. The reduction in the F(2s) signal, the increase in the F(2p) signal, and the large increase in the Cs(5s) signal indicate the formation of cesium fluoride. The formation of cesium fluoride is accompanied by the conversion of the positive electron affinity (PEA) surface to an negative electron affinity (NEA) surface.

The binding energy position of both Cs(5s) and F(2p) shifts approximately 4 eV at cesium saturation coverage; this shift is either due to charging and/or band bending. Band bending is more probable since the diamond crystal is a Type IIB, boron-doped diamond. Moreover, sample charging was not previously observed on the fluorinated surface without cesium. The large increase in downwards band bending was induced by the formation of cesium fluoride. This large increase resulted in transformation of a surface with a very large positive electron affinity (see Table 2) to an NEA surface, as shown in Figure 29. In the case of the fluorinated diamond surface, significantly larger coverages of cesium were reached as shown in Figure 30. The larger coverage was due to the enhanced reactivity of cesium with fluorine (as compared to hydrogen).

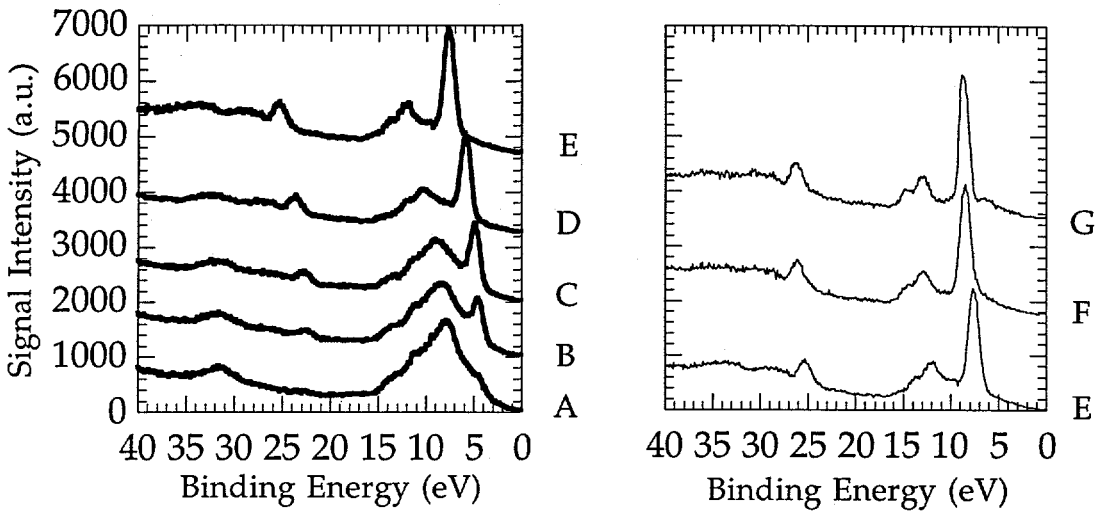

Figure 28 - VB spectrum of fluorinated diamond surface following cesium deposition to saturation vs cesium exposure time (minutes): A)2 B)6; C)10; D)15; E)20; F) 25; and G)32.5. Note the movement of the fluorine core level peaks and the production of the intense, sharp F(2p) (≈5-8 eV) peak in the VB. This peak confirms the presence of cesium fluoride.

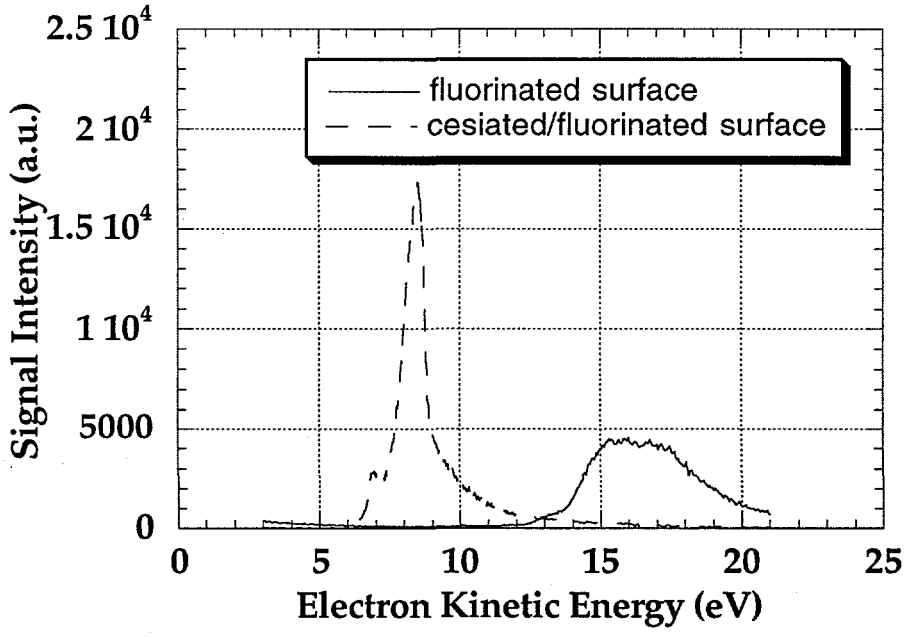

Figure 29 - EDC following cesium saturation on the fluorinated C(110) diamond surface. Note the dramatic reduction in the work function and the formation of a negative electron affinity surface following cesiation.

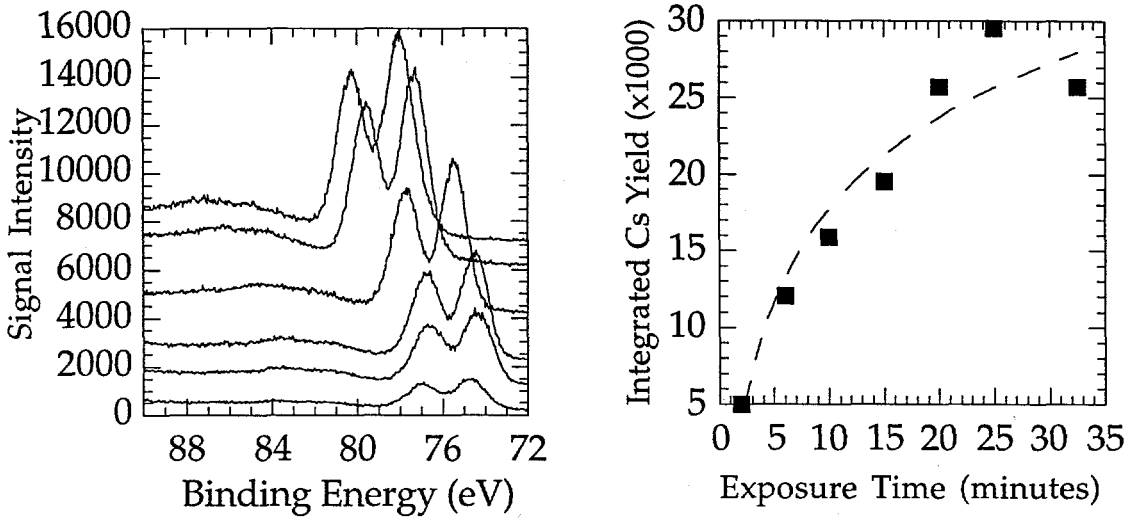

Figure 30 - Cesium core level spectra and integrated yield during cesium deposition. Note the substantially large cesium coverage on the diamond surface compared with the hydrogenated surface.

Thermal Desorption Spectra of Cesium from Diamond Surfaces

Following annealing of the cesiated/fluorinated diamond surface, cesium fluoride desorption occurs. VB spectra and Cs(4d) spectra are shown in Figure 31 as a function of annealing temperature for the cesiated, fluorinated C(110) surface. Cesium fluoride desorption occurs in the temperature range of 100-300°C. Above 300°C, the fluorine concentration is negligible as evidence by the absence of either the F(2s) or F(2p) features. Remnant cesium on the C(110) surface was confirmed by the Cs(4d) spectra shown in Figure 31. These results show that cesiation of fluorinated diamond surfaces is a low-temperature means of depositing cesium onto bare diamond surfaces.

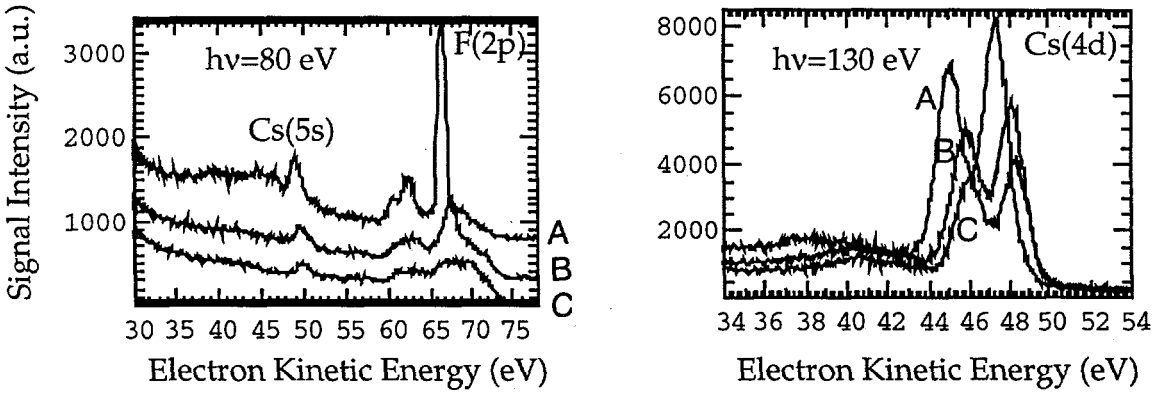

Figure 31 - VB, Cs(4d) spectra vs annealing for fluorinated C(110) surface: A)initial, B)200°C, C)300°C.

Field Emission from Cesiated Diamond-like carbon surfaces

Field emission was measured from a nitrogen-doped diamond-like carbon film following cesiation. Here, a nitrogen-doped DLC was used in lieu of a diamond film due to the inability to dope diamond films n-type. Nitrogen is postulated to act as an n-type dopant in diamond-like carbon films as these films have a significantly higher conductivity when nitrogen is introduced into the growth environment. In this experiment, field emission was measured from three DLC samples (all from same growth run): untreated DLC, cesiated DLC, and cesiated/fluorinated DLC. Field emission maps are shown in Figures 32a, b and c. Note, the emission current intensity scale in Figure 32a is approximately a thousand times more sensitive than those in the latter two plots. The indicated signals are from noise. One can see a substantial increase in the site density was observed for the cesiated/fluorinated sample. This is especially promising as a field emission cathode since the sample was air transferred to the field emission chamber following cesiation (suggesting an air-stable cathode). The bonding of cesium to carbon surfaces in this manner will be discussed in further detail in subsequent papers and a patent application has been written based on this technology.

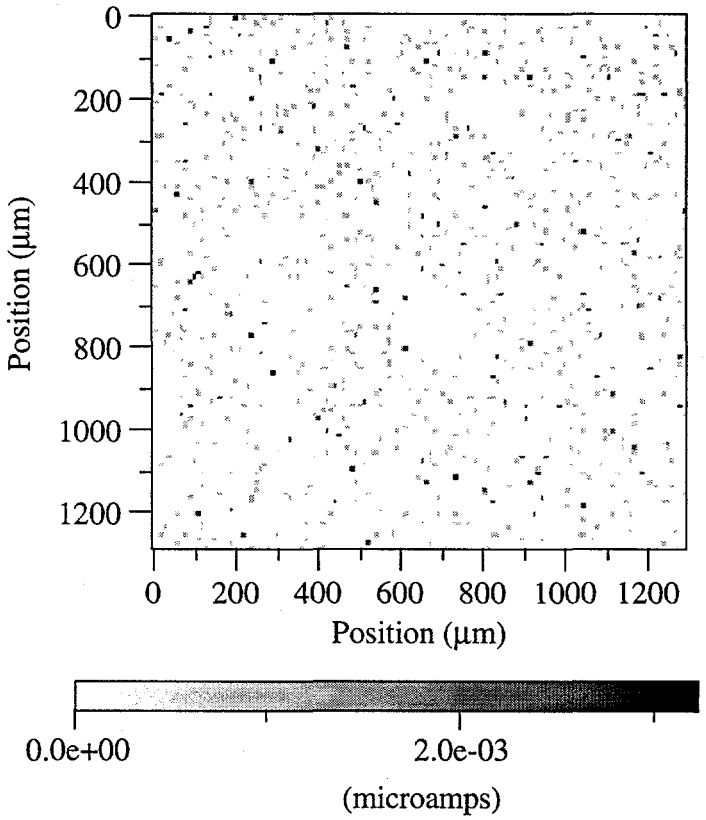

Figure 32a - Field emission map of untreated nitrogen-doped DLC film. Note that no emission sites were observed at an electric field of 125 V/μm.

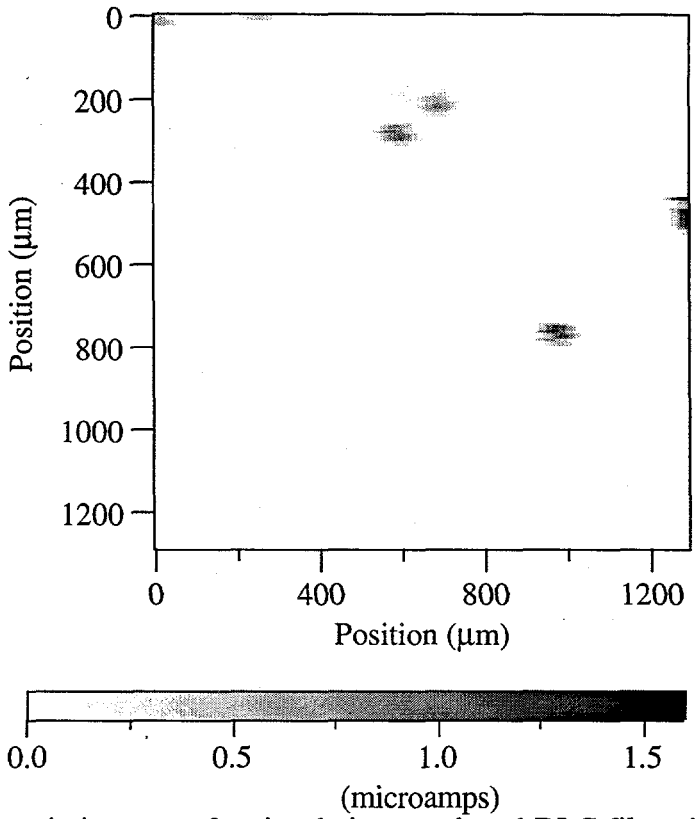

Figure 32b - Field emission map of cesiated nitrogen-doped DLC film. The emission map was measured using an electric field of 95 V/µm.

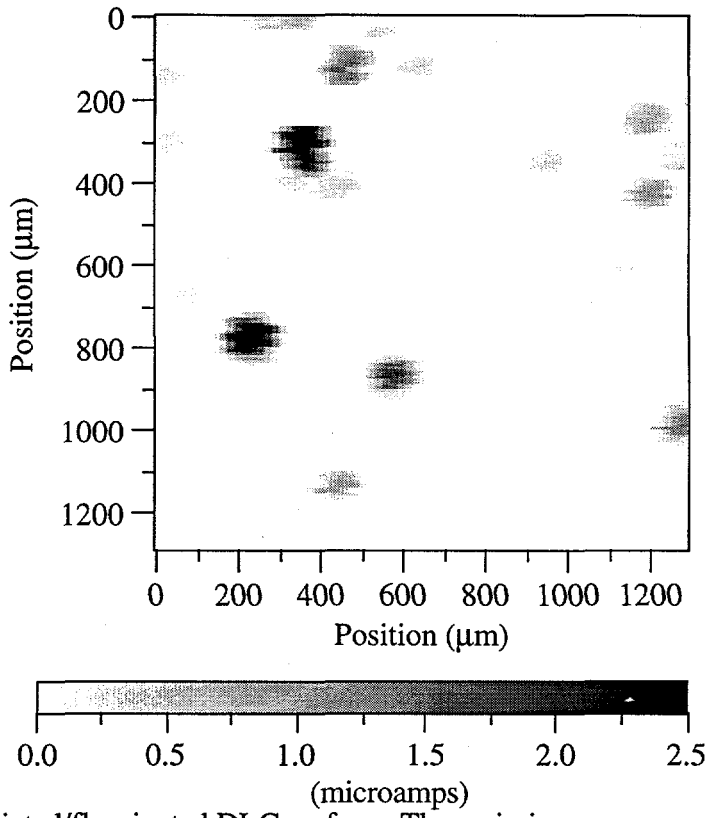

Figure 32c - Cesiated/fluorinated DLC surface. The emission map was measured using an electric field of 61 V/μm.

CONCLUSION

Diamond films were grown using a mixture of fluorocarbons and hydrogen in a conventional microwave plasma deposition system. The use of fluorine and hydrogen simultaneously was based on the enhanced abstraction kinetics of hydrogen and fluorine, respectively. Unfortunately, gas phase reaction to form hydrofluoric acid inhibited simultaneous transport of atomic fluorine and atomic hydrogen to the growing diamond surface. Both the flow tube reactor and the sequential reactor were used to transport atomic hydrogen and atomic fluorine to the growth surface but each achieved limited success. These results show that transport of both the halogen species and atomic hydrogen to the growth surface is the principal limitation to the proposed hybrid diamond growth process.

Although fluorine transport to the diamond surface was limited, ex-situ fluoridation of diamond surfaces was shown to be a viable route toward low-temperature cesiation of diamond surfaces. Using a fluorinated diamond surface, cesium was deposited onto the surface resulting in an NEA surface. In the temperature range of 100-300°C, cesium fluoride desorbed from the diamond surface leaving remnant cesium. Field emission measurements from diamond-like carbon films showed significant enhancement in the emission site density and a simultaneous reduction in the turn-on voltage for cathodes prepared using this procedure.

Acknowledgments

The authors would like to acknowledge the following people for helpful and stimulating discussions:

Robert Hwang, Duanne Outka, Greg Evans, Mark Devyln, Steve Guthrie, Piero Pianetta, and William Spicer.

Funds were provided by the Sandia LDRD program.

Bibliography

1. W. Zhu, B. R. Stoner, B. E. Williams and J. T. Glass, *Proceedings of IEEE* **79** (1991).

2. H. Shiomi, Characterization of Diamond Films and their Application for Electrical Devices, Stanford University, 1993, p. 2.

3. C. Bandis and B. B. Pate, *Physical Review Letters* **74** (1995) 777.

4. M. W. Geis and R. J. Nemanich, in *Fall Materials Research Society Meeting*, Boston, Ma, 1995.

5. P. K. Baumann and R. J. Nemanich, *Diamond and Related Materials* **4** (1995) 802.

6. S. P. McGinnis, M. A. Kelly and S. B. Hagstrom, *Applied Physics Letters* **66** (1995) 3117.

7. B. R. Stoner, S. R. Sahaida, J. P. Bade, P. Southworth and P. J. Ellis, *J. Mater. Res.* **8** (1993) 1334.

8. S. D. Wolter, B. R. Stoner, J. T. Glass, P. J. Ellis, D. S. Buhenko, C. E. Jenkins and P. Southworth, *Appl. Phys. Lett.* **62** (1993) 1215.

9. B. R. Stoner, B. E. Williams, S. D. Wolter, K. Nishimura and J. T. Glass, *J. Mater. Res.* **7** (1992) 257.

10. T. I. Hukka, R. E. Rawles and M. P. D'Evelyn, *Thin Solid Films* **225** (1993).

11. R. Gat, T. I. Hukka and M. P. D'Evelyn, *Proc. 3rd Int. Symp. Diamond Materials (The Electrochemical Society)* (1993).

12. D. E. Patterson, C. J. Chu, B. J. Bai, Z. L. Xiao, N. J. Komplin, R. H. Hauge and J. L. Margrave, *Diamond and Related Materials* **1** (1992) 768.

13. C. Pan, C. J. Chu, J. L. Margrave and R. H. Hauge, *J. Electrochem. Soc.* **141** (1994) 3246.

14. M. G. Wensell, Z. Zhang and J. Bernolc, *Physical Review Letters* **74** (1995) 4875.

15. R. A. Rudder, G. C. Hudson, J. B. Posthill, R. E. Thomas and R. J. Markunas, *Applied Physics Letters* **59** (1991) 791.

16. M. Kadono, T. Inoue, A. Miyanaga and S. Yamazaki, *Appl. Phys. Lett.* **61** (1992) 772.

17. H. Maeda, M. Irie, T. Hino, K. Kusakabe and S. Morooka, *Diamond and Related Materials* **3** (1994) 1072.

18. A. Freedman, *J. Appl. Phys.* **75** (1994) 3112.

19. S. J. Harris, *Applied Physics Letters* **56** (1988) 2298.

20. H. Toyoda, M. A. Childs, K. L. Menningen, L. W. Anderson and J. E. Lawler, *J. Appl. Phys.* (1993).

21. W. Piekarczyk and P. S., *Diamond and Related Materials* **3** (1993) 66.

22. A. Freedman and C. D. Stinespring, in *Second International Conference on New Diamond Science and Technology*, edited by R. Messier, J. T. Glass, J. E. Butler and R. Roy, (Materials Research Society, Washington, D.C., 1991), p. 321.

23. A. V. Hamza, G. D. Kubiak and R. H. Stulen, *Surf. Sci.* **237** (1990) 35.

24. M. T. Schulberg, C. A. Fox, G. D. Kubiak and R. H. Stulen, *J. Appl. Phys.* **77** (1995).

25. M. T. Schulberg, G. D. Kubiak and R. H. Stulen, *J. Appl. Phys.* **77** (1995) 3484.

26. L. H. Chua, R. B. Jackman, J. S. Foord, P. R. Chalker, C. Johnston and S. Romani, *J. Vac. Sci. Technol. A* **12** (1994) 3033.

27. D. D. Koleske, S. M. Gates, B. D. Thoms, J. N. J. Russell and J. E. Butler, *J. Chem. Phys.* **102** (1995) 992.

28. D. D. Koleske, S. M. Gates, B. D. Thoms, J. N. J. Russell and J. E. Butler, *Surface Science Letters* **320** (1994) L105.

29. N. J. Komplin, B. J. Bai, C. J. Chu, J. L. Margrave and R. H. Hauge, in *Third International Symposium on Diamond Materials, ECS*, edited by J. P. Dismukes and K. V. Ravi, (The Electrochemical Society, Hawaii, 1993), vol. 93-17, p. 385 .

30. D. E. Patterson, B. J. Bai, C. J. Chu, R. H. Hauge and J. L. Margrave, in *Second International Conference on New Diamond Science and Technology*, edited by R. Messier, J. T. Glass, J. E. Butler and R. Roy, (Materials Research Society, Washington, D.C., 1991), p. 433 .

31. H. F. Winters and J. W. Coburn, *Surface Science Reports* **14** (1992) 161.

32. D.-W. Kweon, J.-Y. Lee and D. Kim, *J. Appl. Phys.* **69** (1991) 8329 .

33. M. C. McMaster, W. L. Hsu, M. E. Coltrin and D. S. Dandy, *J. Appl. Phys.* **76** (1994) 7567.

34. T. Mitomo, E. Kondoh and K. Ohtsuka, *J. Appl. Phys.* **70** (1991) 4532.

35. B. J. Bai, C. J. Chu, D. E. Patterson, R. H. Hauge and J. L. Margrave, *J. Mater. Res.* **8** (1993) 233.

36. M. A. Kelly, D. A. Olson, S. Kapoor and S. B. Hagstrom, *Applied Physics Letters* **60** (1992) 2502.

37. W. E. Pickett, *Physical Review Letters* **73** (1994) 1664.

38. M. W. Geis, J. C. Twichell, J. Macaulay and K. Okano, *Appl. Phys. Let.* **67** (1995) 1328.

39. G. T. Mearini, I. L. Krainski, J. A. Dayton, Y. X. Wang, C. A. Zorman, J. C. Angus, R. W. Hoffman and D. F. Anderson, *Appl. Phys. Lett.* **66** (1995) 242.

40. G. T. Mearini, I. L. Krainski, J. A. Dayton, Y. X. Wang, C. A. Zorman, J. C. Angus and R. W. Hoffman, *Appl. Phys. Lett.* **65** (1994) 2702.

41. A. Freedman and C. D. Stinesspring, *Appl. Phys. Lett* **57** (1990) 1194.

42. M. E. Coltrin, R. J. Kee, and G. H. Evans, *J. Electrochem. Soc.*, **136,** 819 (1989).

43. M. E. Coltrin, R. J. Kee, and F. M. Rupley, *Int. J. Chem. Kinet.*, **23,** 1111 (1991).

44. R. J. Kee, F. M. Rupley and J. A. Miller, Sandia Laboratories Report, SAND89-8209 (1989).

45. M. E. Coltrin and D. S. Dandy, *J. Appl. Phys.*, **74,** 5803 (1993).

46. M. C. McMaster, W. L. Hsu, M. E. Coltrin and D. S. Dandy, *J. Appl. Phys.*, **76,** 7567 (1994).

47. D. S. Dandy and M. E. Coltrin, *J. Appl. Phys.*, **76,** 3102 (1994).

48. H. N. Chu, E. A. Den Hartog, A. R. Lefkow, J. Jacobs, L. W. Anderson, M. G. Lagally, and J. E. Lawler, *Phys. Rev. A*, **44,** 3796 (1991).

49. W. A. Weimer, F. M. Cerio, and C. E. Johnson, *J. Mater. Res.*, **6,** 2134 (1991).

50. A. E. Lutz, R. J. Kee and J. A. Miller, Sandia Laboratories Report, SAND87-8248 (1988).

51. N. L. Allinger, Y. H. Yuh, and J.-H. Lii, *J. Amer. Chem. Soc.*, **111,** 8551 (1989).

52. N. L. Allinger, Y. H. Yuh, and J.-H. Lii, *J. Amer. Chem. Soc.*, **111,** 8566 (1989).

53. N. L. Allinger, Y. H. Yuh, and J.-H. Lii, *J. Amer. Chem. Soc.*, **111,** 8576 (1989).

54. B. C. Garrett and D. G. Truhlar, *J. Amer. Chem. Soc.*, **101,** 5207 (1979)

55. M. E. Coltrin, estimated.

56. K. Sugawara, T. Nakanaga, H. Takeo, and C. Matsumura, *Chem. Phys. Lett.*, **134,** 347 (1987).

57. C. Tsai and D. L. Mcfadden, *J. Phys. Chem.*, **93,** 2471 (1989).

58. P. K. Chowdhury, K. V. S. Rama Rao, and J. P. Mittal, *J. Phys. Chem.*, **92,** 102 (1988).

59. A. P. Modica, *J. Chem. Phys.*, **44,** 1585 (1966).

60. A. P. Modica and S. J. Sillers, *J. Chem. Phys.*, **48,** 3283 (1968).

61. C. Tsai and D. L. McFadden, *J. Phys. Chem.*, **93,** 2471 (1989).

62. G.B. Skinner and G.H. Ringrose, *J. Chem. Phys.*, **43,** 4129 (1965).

63. J. C. Amphlett and E. Whittle, *Trans. Farad. Soc.*, **63,** 2695 (1967).

64. H.S. Johnston and C. Parr, *J. Chem. Phys.*, **85,** 2544 (1963).

65. D. Raybone, T. M. Watkinson, and J.C. Whitehead, *Chem. Phys. Lett.*, **139,** 442 (1987).

66. R. M. Robertson, D. M. Golden, and M.J. Rossi, *J. Chem. Phys.*, **92,** 5338 (1988).

67. V. F. Kochubei and F. B. Moiri, *Kinet. Catal. (USSR)*, **10,** 405 (1969).

68. N. Cohen and K.R. Westberg, *J. Phys. Chem. Ref. Data*, **12,** 531 (1983).

69. D. L. Baulch, J. Duxbury, S. J. Grant, and D. C. Montague, *J. Phys. Chem. Ref. Data*, **10,** Suppl. 1, 1-1 (1981).

70. R. W. Diesen, *J. Chem. Phys.*, **44,** 3663 (1966).

71. *Pyrodynamics*, **4,** 371 (1966).

72. G. Dixon-Lewis, *Philos. Trans. R. Soc. London Ser. A,* **303,** 181 (1981).

73. R. A. Svehla, NASA Report, NASA-TR 132 (1962).

UNLIMITED RELEASE

INITIAL DISTRIBUTION:

MS 0188 C. E. Meyer, 4523 (LDRD Office)
MS 0333 Alan Hurd, 1841
MS 0340 Mike Dugger, 1832
MS 0340 Diane E. Peebles, 1832
MS 0342 R. J. Salzbrenner, 1805
MS 0367 Brian Dankroger, 1833
MS 0367 Richard J. Buss, 1812
MS 0513 R. J. Eagan, 1000
MS 0601 M. E. Coltrin, 1126
MS 0603 Peter E. Esherick, 1314
MS 0957 Janda Panitz, 1411
MS 0985 M. W. Callahan, 5202
MS 1056 Barney L. Doyle, 1111
MS 1056 David S. Walsh, 1111
MS 1056 William R. Wampler, 1111
MS 1078 Charles W. Gwyn, 1302
MS 1078 David R. Myers, 1303
MS 1079 A. D. Romig, 1300
MS 1082 James Sweet, 1333
MS 1405 Thomas J. Headley, 1822
MS 1405 Clifford Renschler, 1812
MS 1421 John P. Sullivan, 1153
MS 1421 Tom Friedman, 1153
MS 1421 Ellen B. Stechel, 1153
MS 1421 Michael P. Siegal, 1153
MS 1421 George A. Samara, 1152
MS 1423 Paul A. Miller, 1128
MS 1423 Gerald N. Hays, 1128
MS 1427 S. Thomas Picraux, 1100
MS 1434 Gordon E. Pike, 1802
MS 1435 Harry J. Saxton, 1800
MS 9001 T. O. Hunter, 8000;
Attn: J. B. Wright, 2200
M. E. John, 8100
L. A. West, 8200
W. J. McLean, 8300
R. C. Wayne, 8400
P. N. Smith, 8500
P. E. Brewer, 8800
D. L. Crawford, 8900
MS 9007 Arthur Pontau, 8801
MS 9012 Les Brown, 8930
MS 9052 Mark D. Allendorf, 8361
MS 9052 Donald R. Hardesty, 8361
MS 9053 David W. Hahn, 8366
MS 9056 Robert J. Gallagher, 8366

MS 9161	Kevin McCarthy, 8342
MS 9161	W. G. Wolfer 8717
MS 9161	John Weeks, 8230
MS 9161	Steve Bosson, 8716
MS 9161	K. L. Wilson, 8716
MS 9201	W. L. Hsu, 8112 (20)
MS 9402	Steven E. Guthrie, 8715
MS 9402	George J. Thomas, 8715
MS 9402	Nancy Yang, 8715 (5)
MS 9402	Lawrence Pan, 8715
MS 9402	Tom Felter, 8715
MS 9403	David K. Ottesen, 8713 (5)
MS 9403	Jim C. F. Wang, 8713
MS 9405	Jill M. Hruby, 8230
MS 9405	Ralph James, 8230
MS 9405	Michael T. Dyer, 8700
MS 9409	Richard H. Stulen, 8250

MS 9021	Technical Communications Department, 8815 for OSTI (10)
MS 9021	Technical Communications Department, 8815/Technical Library, MS 0899, 4414
MS 0899	Technical Library, 4414 (4)
MS 9018	Central Technical Files, 8940-2 (3)